Master's thesis

NTNU
Norwegian University of Science and Technology
Faculty of Natural Sciences
Department of Materials Science and Engineering

Andrés Greciano Zamorano

Modeling and performance analysis of a solar photovoltaic energy community in Norway

Master's thesis in Innovative Sustainable Energy Engineering: Solar Cell Systems and Materials
Supervisor: Marisa Di Sabatino (NTNU) and Sergiu Viorel Spataru (DTU)
Co-supervisor: Steve Völler (NTNU) and Anders Eidberg (EIDA Energy)
June 2023

NTNU
Norwegian University of Science and Technology

Andrés Greciano Zamorano

Modeling and performance analysis of a solar photovoltaic energy community in Norway

Master's thesis in Innovative Sustainable Energy Engineering: Solar Cell Systems and Materials
Supervisor: Marisa Di Sabatino (NTNU) and Sergiu Viorel Spataru (DTU)
Co-supervisor: Steve Völler (NTNU) and Anders Eidberg (EIDA Energy)
June 2023

Norwegian University of Science and Technology
Faculty of Natural Sciences
Department of Materials Science and Engineering

NTNU
Norwegian University of
Science and Technology

Acknowledgments

This Master's thesis is probably the last step of my university educational training, and I suppose it closes a great stage of my life. I feel really fortunate and proud of having followed the educational path I chose, which in the end is educational in many ways. This university journey started in September 2015 with me commuting from home to Escuela de Caminos, Canales y Puertos to attend the Material's Science Engineering welcome session, and ends with me heading back home from Trondheim after defending this Master's thesis and enjoying this amazing country for the last few days. In between there are countless hours of studying and enriching experiences with multiple people and in multiple places. This would not have been the same without:

- My parents, Emilio and Elena, and brother, Emilio, for their constant support, trust in me and convenient advice.
- My girlfriend, Ana, for having keenly shared with me these last two years.
- The friends I met during these years, for their quality company on and off campus, including Diego, Marcos, Marti, Ricky, Peri, Raúl, Victor, Lennart, Sarah, Isabella, Heather, Aurélian, Harry, Joseba, Vilma, Sarah, Jacob and Ahmad.
- The professors that shared their knowledge with eagerness, kindness and empathy, trying to understand the students' concerns.

I would like to express my gratitude to the universities in which I studied and some specific professors:

- UPM (Madrid), for being my proudly home university. Thanks to the supervisors of my Bachelor's thesis, José Luis Prieto and Marco Maicas, for being good examples of what is written above about professors. Thanks as well to Alejandro Datas for his valuable advice just before starting this Master's degree.
- INSA (Rennes), for kindly hosting me during my Erasmus and being my main inspiration to go deeper into renewables and photovoltaics. Thanks to Mathieu Perrin for his dedication and patience.
- DTU (Lyngby) and NTNU (Trondheim), for having set up this joint Nordic Master's degree program on Solar energy, which is unique. Thanks to my NTNU and DTU supervisors, Marisa Di Sabatino and Sergiu Viorel Spataru, and NTNU co-supervisor, Steve Völler, for having guided me throughout this semester to complete this Master's thesis.

I am also grateful to the company EIDA Energy for always being open to collaborate in the Master's thesis. More specifically, thanks to my co-supervisor, Anders Eidberg, and Kenneth Dallager.

Todo pasa y todo queda,
pero lo nuestro es pasar,
pasar haciendo caminos,
caminos sobre la mar.

Golpe a golpe, verso a verso.

Abstract

The high electricity prices, falling PV installation costs, and high expectation on PV energy to be, together with wind energy, the main pathways to reach the European Net Zero Emission (NZE) goal by 2050, is causing increasingly larger amounts of PV installations worldwide. This high PV penetration and the nature of solar energy can overload and imbalance the grid network with large amounts of surplus PV energy generated at certain times of the day and year when the PV generation exceeds the electricity demand. In this context, self-consumption solutions have to be found that enable consuming most of the generated PV energy while still covering a large share of the electricity demand. One of these possible solutions is the implementation of energy sharing in residential PV energy communities (ECs), which is a currently researched novel concept already suggested by the EU directives [1]. Energy sharing among prosumers in an EC scheme improves energy efficiency over having individual buildings with no energy sharing. Taking advantage of the multiple tilts and orientations of the different buildings forming the EC enhances even more the energy efficiency by matching even further the PV generation with the load consumption (load-match). This is something rarely studied by the scientific community.

In this report a PV sizing optimization model is developed in Excel. The model uses as input PV generation data from the software SAM and load consumption data from the software Load Profile Generator. The data obtained from these two softwares is inputted in Excel. Excel is used to define and solve the sizing optimization problem. The Excel solver "GRG Nonlinear with multistart" is used to find the optimal PV capacities for certain battery capacity sizes and energy goals based on self-consumption metrics, such as the self-consumption rate (SCR), the self-sufficiency rate (SSR) and the energy balance index (EBI). The model is validated by comparing its results with results from the software SAM and by using two different optimization solver algorithms in Excel: "GRG Nonlinear with multistart" and "Evolutionary". The model is specifically applied to an upcoming residential PV EC formed by 100 households in Harstad, Norway [2]. Results show that an optimal EC PV sizing must consider all possible surfaces with different orientations and tilts. While a tilt of 60° is dominant (among 0°, 20°, 40° and 60°) due to the specific Nordic location, all different orientations considered (E,W,S,N) are used for optimal PV installation. High levels of electricity demand coverage (high SSR) are achieved with relatively low PV capacities on high PV output orientations, such as south, but when a considerably high load-match has been achieved for the PV energy produced from these high PV output orientations, it is reasonable to cover the remaining electricity demand with PV energy from north and west orientations, causing small amounts of surplus energy (high SCR).

Table of contents

1 Background

1.1 Climate change and electrification

Climate change refers to the long-term alteration of global weather patterns, primarily caused by human activities such as the burning of fossil fuels and deforestation, which release large amounts of greenhouse gases (GHG) into the atmosphere. These emissions trap heat and contribute to the warming of the planet, leading to significant implications for our planet, including rising sea levels, increased frequency and intensity of natural disasters, and disruption of ecosystems and wildlife. In addition to these environmental impacts, GHG emissions also have severe consequences for human health, such as respiratory illnesses from air pollution and exposure to toxic substances. While climate change has been occurring for many years since the start of the Industrial Revolution in the 19th century, it has accelerated significantly in recent decades, as observed in Figure 1. This is due to a combination of factors, including population growth, increased industrialization and higher standards of living. These factors have caused a rapid increase in GHG emissions from human activities, making the need to take action against climate change more urgent than ever before.

Figure 1 shows the clear correlation between the rise of carbon dioxide (CO2) levels, main GHG contributor to global warming, and the increase in global temperature, since 1880 through 2012. While there is a clear long-term global warming trend due to GHG emissions, especially from 1980 on, some years do not show a temperature increase relative to the previous year, and some years show greater changes than others. These year-to-year fluctuations in temperature are due to natural processes, such as the effects of El Niño, La Niña, and volcanic eruptions [3].

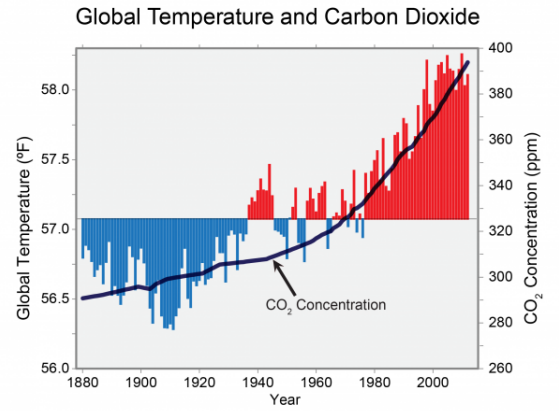

Figure 1: Global annual average temperature (blue and red columns) and CO2 concentration (dark blue line) since 1880 through 2012. Red bars show temperatures above the long-term average, and blue bars indicate temperatures below the long-term average [3].

Figure 1 shows data until 2012. However, the situation has not improved in the last decade. Despite the last two years (2021 and 2022) not ranking among the five warmest years on record, the 10 warmest years have all occurred since 2010, with the last nine years (2014–2022) ranking as the nine warmest years on record [4]. Governments and organizations around the world have recognized the urgent need to combat climate change and have begun implementing policies and measures to address this global issue. The Paris Agreement is an international treaty adopted in 2015 by 196 countries, with the goal of limiting global warming to less than 2°C above pre-industrial levels and to pursue efforts to limit the temperature increase to 1.5°C [5]. The Intergovernmental Panel on Climate

Change (IPCC) has underlined that a warming of close to 2°C would still entail strong negative impacts for societies around the world so the current goal, agreed again in Glasgow at COP26 in 2021 [6], is to limit the temperature increase to 1.5°C [7]. Policy and technology changes since the Paris Agreement in 2015 have reduced the projected temperature rise, but there remains a huge amount to be done, particularly in emerging market and developing economies. It is reminded that this is a global issue.

The European Union (EU) has a strong influence on climate policies and has set ambitious goals in recent years, which have been augmented several times. In January 2020, the European Parliament introduced the European Green Deal, an action plan to boost the efficient use of resources by moving to a clean, circular economy and to restore biodiversity and reduce pollution [8]. The main goal of the European Green Deal is to become a global economy with net-zero GHG emissions (NZE) by 2050. This is an ambitious goal deemed as necessary to limit the temperature increase to 1.5°C. To this end, in June 2021 the European Comission established a target reduction of 55% GHG emissions by 2030 compared to 1990 levels, the so-called "Fit for 55" goal [9]. To date, over 90 countries and 78.7% of global GHG emissions have committed to the NZE objective [10]. The goal pursues that all countries in the world, not only European countries, reach NZE by 2050, but not necessarily at the same time, neither the time frame for reaching NZE is the same for CO2 alone, which is the main GHG, than for CO2 plus other GHG, such as methane, nitrous oxide and fluorinated gases. However, it is clear that the chances of limiting global warming to 1.5°C depend significantly on how soon action is taken.

The energy sector is responsible for a major part of the global GHG emissions, with energy-related emissions evaluated at 33 Gt $CO2_{eq}$ in 2021. $CO2_{eq}$ stands for "Carbon Dioxide Equivalent" and measures CO2 emissions plus all other GHG emissions. Within the energy sector, the electricity (power) sector emitted 13 Gt CO2 emissions in 2021, which represents more than one-third of the global energy-related CO2 emissions. Figure 2 shows the electricity mix in 2021. It is observed that it is mainly based on fossil fuels sources. The EU has historically supported high renewable energy (RE) developments to tackle climate change. The share of RE in the EU's final energy consumption has been targeted to 45% by 2030. In 2022, the REPowerEU has been proposed as a joint European action for more affordable, secure, and sustainable energy to accelerate the energy transition and to secure the EU's energy supply and disconnect Europe from Russian gas and oil imports. REPowerEU includes short and medium-term milestones which aim at a full independence from all Russian energy imports by 2027, given the ongoing conflicts in Ukraine and the EU's stance towards Russia. The plan would bring the total RE generation capacities to 1236GW by 2030, in comparison to the original "Fit for 55" 1067GW planned by 2030. This plan will be paving the way for an era of RE at affordable prices while accelerating their development. It aims at achieving energy savings, produce clean energy and diversify the EU's energy supply sources [11] [12].

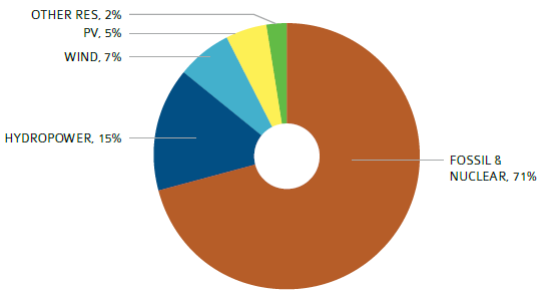

Figure 2: Energy sources used in electricity production in 2021 [11].

Clean electricity from RE not only cuts emissions in the electricity sector itself but also in other energy end-use sectors, such as space heating/cooling, transport or industrial processes, as they look to electricity as the energy source alternative to fossil fuels. As a result, electricity becomes the "new oil" in terms of its dominant role in final energy consumption. This is why a huge overall increase in global electricity demand is expected over the coming decades. The success of this electrification depends on modern electricity grid networks, and their development requires long-term vision and planning. To ensure security of supply, grid development must be considered at the system level, taking account of increasing electricity demand and rising levels of variable RE [12].

Global electricity generation increases over two-and-a-half-times from 2021 to 2050 in the International Energy Agency (IEA) hypothetical NZE Scenario published in October 2022, a narrow but achievable pathway for the global energy sector to achieve NZE by 2050. It sees all countries contribute to this global goal, with advanced economies taking the lead and reaching NZE well before emerging market and developing economies. The aforementioned electrification of several end-use sectors raises the share electricity in final consumption from 20% in 2021 to almost 30% in 2030, and more than 50% in 2050. RE rapidly becomes the foundation of the global electricity sector in the NZE Scenario. The share of RE in electricity generation rises from 28% in 2021 to over 60% in 2030, and nearly 90% in 2050. Solar photovoltaic (PV) energy and wind energy are the leading means of cutting electricity sector emissions: their global share of electricity generation increases from 10% in 2021 to 40% by 2030, and 70% by 2050, as shown in Figure 3 [12].

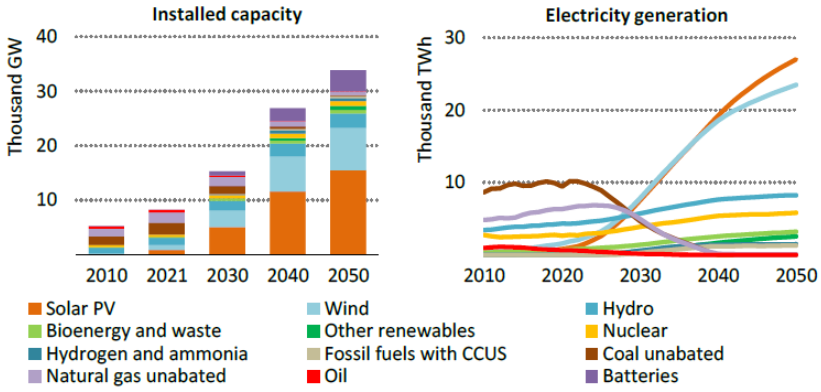

Figure 3: Total installed capacity (left) and electricity generation (right) by source in the NZE Scenario, 2010-2050. Total electricity generation nearly triples to 2050, with a rapid shift away from unabated coal and natural gas to low-emissions sources, led by solar PV and wind [12].

The NZE Scenario is an ambitious and possible pathway to reach NZE by 2050, but not the only one. Published in April 2022, the third volume of the IPCC Sixth Assessment Report deals with climate mitigation. Among the more than 1000 scenarios vetted by the IPCC, only 16 achieved NZE by 2050, and are therefore comparable with the IEA NZE Scenario. The IEA NZE Scenario entails very ambitious policies and measures to improve energy efficiency and reduce energy demand, including through behavioural change. As a consequence of this and the benefits of electrification, total final consumption is around 340 EJ in 2050, compared to around 460 EJ in the median IPCC scenario. Moreover, the NZE Scenario sees the share of wind and solar in electricity generation reach over 70% in 2050, compared to around 55% in the median IPCC scenario. Still, it is clear that a clean electrification is absolutely central to the shift to a NZE economy and that the implementation of solar PV and wind will be the cornerstones in the energy transition [12].

1.2 PV market

A large PV share in the electricty mix can significantly reduce the emissions from power generation. The global average carbon intensity of electricity was around 475 g CO2/kWh in 2019 whereas for 1 kWh produced by PV the emitted CO2 considered on a life cycle basis can be as low as 15g depending on technology and irradiation conditions. At the end of 2021, the global PV installed capacity was 945GW. This capacity represents around 5% of the global electricity production, as shown in Figure 2. As part of the aforementioned REPowerEU plan, the EU Solar Energy Strategy's aim is to boost the roll-out of PV energy. This strategy aims to bring online over 320 GW of solar PV capacity by 2025, and almost 600 GW by 2030 [11].

Figure 4 shows the amount of cumulative PV installed per capita worldwide at the end of 2021. In just a few years, Australia has reached the highest installed PV capacity per inhabitant with 1011 W/cap, followed by The Netherlands with 818 W/cap, Germany with 718 W/cap, Japan with 622 W/cap and Belgium with 620 W/cap. As a comparison, since 500W represents the power of a large PV module, one can say that in some countries one module per person has been installed. In terms of installed PV capacity, the ten first countries cover around 78% of the global PV market. China covers more than one third of the global market and has been in the first place year to year since 2013. Moreover, the level of installations required to be included in the yearly top 10 (country wise) has increased steadily: from 0,78 GW in 2014 to 1,6 GW in 2018, and around 3,5 GW in 2020 and 2021. This reflects the global growth trend of the solar PV market [11].

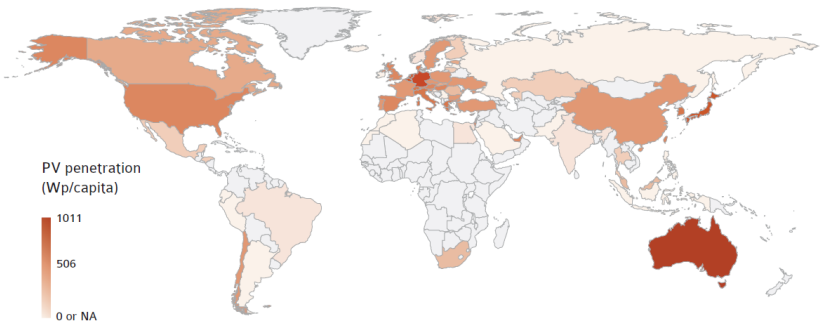

Figure 4: PV penetration per capita in 2021 [11]

In the first years of this century, Europe led PV development for years and represented more than 70% of the global cumulative PV market until 2012. PV systems were profitable due to highly subsidized feed-in tariffs (FiTs) which were implemented to promote the ongoing decarbonization. Several European countries experienced PV market booms caused by an unpredictable and steep decrease of PV system costs and a not proper adjustment of FiTs, which remained excessively high. This situation caused the market to grow out of control. Unfortunately, these booms strained the subsidies budget and negatively affected the public perception of PV. Most of these markets took years to recover and reexperience growth. From 2013 to 2017, European PV installations decreased while there was rapid growth in the rest of the world, mainly in Asia and the Americas. Therefore, many countries in Europe adopted the principle of decreasing FiT levels over time or introduced limited budgets [13] [11].

However, since 2018 the situation improved gradually in most European countries and PV installations rose in Europe. Falling PV systems installation costs, the increase in energy costs in 2021 and 2022, specifically electricity prices, and the climate policies to reach NZE

by 2050 have enhanced PV attractiveness in numerous countries. If high electricity prices remain, the question of competitiveness will change completely as will the way to conceive PV market support and policy framework. With no need of any support schemes, the PV market potential looks virtually unlimited. However, targeted financial incentives are still needed to overcome costs or investment barriers in specific countries or regions with weak sunlight or low electricity prices. Predefined FiTs in centralized (utility-scale) PV are being replaced in many countries by auctions with calls for tenders to propose the most competitive PV electricity. Support for the distributed (residential and commercial) PV market often relies on FiTs, which still supported half of these segments in 2021 (54%), even if the trend leans towards lower FiTs [11]. In the distributed market, lower FiTs have come together with a decrease in the net energy (energy generated minus energy consumed) metering interval time, turning from longer periods, using the grid as an energy storage unit, into an real-time metering scheme in most countries. The longer the metering period the more likely is to compensate with own surplus PV energy the times with not enough PV generation, not having to buy energy from the grid and hence increasing profitability.

The share of utility-scale still represented around 55% of cumulative installed PV capacity in 2021. With the exception of the European market which incentivized residential segments from the start, initially most of the major PV developments in emerging PV markets are coming from utility-scale PV. Utility-scale PV requires developers and financing institutions to set up plants in a relatively short time. This option allows the start of using PV electricity in a country faster than what distributed PV requires. Moreover, tenders are making PV electricity even more attractive in some regions. Economies of scale in utility-scale PV outweigh the savings in transmission costs and the self-consumption possibilities brought by distributed installations. However, both trends are compatible as some policies were implemented recently in emerging markets to incentivize rooftop installations and tenders for rooftop installations are being organized in several historical markets [11].

The European market has incentivized distributed residential segments from the start. Almost 55% of the cumulative capacity installed in the EU at the end of 2021 were residential and commercial rooftop installations [11]. The importance of citizen involvement in the transition of the energy sector towards a decentralized structure has been recognized through different EU Directives, which include new rules that enable active consumer participation (prosumer: producer and consumer), individually or through citizen energy communities (CEC) in all markets, either by generating, consuming, sharing or selling electricity, or by providing flexibility services through demand-response and storage [14] [15].

1.3 High PV penetration

PV penetration is defined as the ratio between PV electricity production and the electricity demand, typically in a country. PV penetration has increased considerably in many countries in recent years and is expected to keep increasing, to reach NZE by 2050. PV energy, similarly to most RE and unlike conventional fossil-fuel based energy, is highly unpredictable and intermittent due to the weather variability. These two factors, high PV penetration and high variability, cause large amounts of surplus PV energy, especially at peak generation times [16] [17].

In this context, a robust and large grid network capacity is needed to store and transmit this surplus energy. Besides grid capacity challenges, grid balancing challenges may also arise since electricity supply needs to exactly match demand at all times (instantaneously) to ensure system stability, avoiding voltage and frequency failures. In other words, exports of solar power from multiple houses simultaneously pose a threat to distribution grids, potentially giving rise to voltage violations (balancing issues) and line overload (capacity issues).

For these two technical reasons [18] [19], together with the decreasing trend of FiTs [13], the focus is no longer on maximizing PV production and using the public grid as a limitless energy storage for surplus energy, but on matching the PV production profile to the load consumption profile and self-consuming on-site and instantaneously the self-generated PV energy, reducing the surplus energy [17]. In this context, 'profile' does not refer as the total amount of energy produced or consumed, but rather to the times of the day and year in which this energy is produced or consumed. In recent years self-consumption regulations are increasingly being implemented in different countries, especially in Europe; the aim is to empower prosumers to play an important role in the energy transition to reach NZE by 2050 [11].

Although self-consumption schemes benefit grid operators by not having to deal with the excessive balancing and capacity issues mentioned above, they will see their revenues and therefore their capacity to invest and maintain the grid reduce significantly, as a result of prosumers becoming semi-independent from the grid and not purchasing as much energy from it. At the same time, since a 100% grid independence is difficult to accomplish, a proper grid availability and maintenance is still needed by prosumers to use the grid as a sink for surplus PV production and as a backup for periods of insufficient PV generation. Therefore, together with the increasing self-consumption incentives, several countries are also accounting for these prosumer's saved grid-costs. The question of grid costs becomes more important with the expected electrification and rising PV penetration and is already leading in some countries to specific tariffs which are reducing the competitiveness of distributed PV installations and self-consumption. In particular, several countries discuss the shift of grid costs from the traditional energy-based structure (price per kWh taken from the grid) towards one that gives more weight to the fixed grid costs. Here, it is observed how important it will be for the grid operators to know their real costs, which requires reasonable long-term planning and a modern network with smart meters. Only with this information grid operators will be able to invoice prosumers with a fair tariff depending on their real use of the grids [11].

1.4 PV self-consumption mechanisms

1.4.1 Storage

Storage is a key element of a carbon neutral energy system relying on RE electricity. Therefore, the European Commission actively supports energy storage through research and innovation funds. The adoption of batteries is on the rise in distributed PV as more and more consumers are willing to maximise their self-consumption and to optimize their consumption profile. Globally, the largest part of batteries sold are used for transportation in Electric Vehicles (EVs), while stationary storage remains the exception and volumes remain small. However, the rapid development of electric mobility is driving battery prices down much faster than any could have expected in the stationary market alone. This could give a huge push to the development of storage as a tool to ease PV installations in some specific conditions [11].

Moreover, the fast development of EVs might change the landscape of distributed PV systems: some consider that storage development for PV electricity will be massively realized through EVs connected to the grid during a large part of the day and therefore, will be able to store and deliver energy to consumers at a larger scale than simple batteries. Clearly, PV and EVs offer a potential synergy, with EV batteries absorbing surplus power from nearby PV installations [19]. This vehicle-to-grid (V2G) concepts are being explored and tested in several countries. However, despite their decreasing costs and subsidies in some countries, battery storage is not yet economically viable in all countries. It is, therefore, questionable

whether small-sized storage systems can already be operated economically without subsidy programs [20]. Therefore, complementary solutions have to be found to deal with high PV penetration.

The required electrification of space heating and cooling to achieve NZE by 2050 creates new opportunities to use solar electricity for specific buildings appliances, increasing self-consumption [13]. Among others, even if the solar electricity production is not directly linked to consumption load in the case of space heating (space heating does not usually rely on electricity as energy source), it is becoming a real source of interest to use surplus PV electricity to feed electric domestic hot water tanks for instance. Hot water tanks can also serve as storage and can be successfully combined with a heat pump [17]. Several European manufacturers of electric domestic hot water tanks are now offering specific electronic devices to directly link extra PV production to an electric boiler. Another very promising segment in the use of solar PV electricity is the use for cooling. Indeed, places where grid stress is very present in summertime, benefiting from solar cooling and cooling thermal storage based on surplus PV production can become a very powerful tool [11].

Curtailment refers to the reduction of RE generation during times of excess supply, resulting in wasted energy and decreased efficiency. It can be achieved through various technical means. This is often seen as a last resort measure to avoid grid stability issues and is generally avoided unless absolutely necessary. However, oversizing PV systems and proactively curtailing when there is surplus energy, a strategy known as "implicit storage", is a novel solution to increase the self-consumption while still covering a large portion of the electricity demand by solar PV. This is seen as a promising concept in IEA [16], providing examples of implicit storage implementations, and stressing other important concepts to achieve high levels of self-consumption, such as optimum blending of different RE sources (PV, wind and hydro) that often exhibit complementary diurnal or seasonal generation profiles, as well as demand flexibility via demand-side management (DSM), which involves shifting electricity consumption (load shifting) to times when self-generated energy is available.

1.4.2 Energy sharing

In the traditional retail market structure, residential PV owners are only able to individually buy and sell energy with electricity retailers. This concept is known as a peer-to-grid (P2G) system. Another possible solution to increase self-consumption is by sharing the energy from different distributed PV systems, allowing the direct energy exchange among different households, typically by means of a micro-grid and forming an energy community (EC), following the scheme in Figure 5. This concept is known as a peer-to-peer (P2P) trading system and is being investigated by numerous authors [21] [20]. Depending on the definition, the EC concept might also include the concept of collective self-consumption, in which one or several PV systems feed collectively several consumers using a predefined split key, typically in a multi-apartment building but also in distinct individual buildings. Here no exchange of energy among the households really occurs, following a P2G mechanism, but the households still share the collective (aggregated) PV generated energy, enhancing energy efficiency. Collective self-consumption exists in Portugal, Spain, Austria, Canada, Sweden, France, Switzerland, Germany or Italy to mention a few [11]. The EC concept may refer rather to a P2P trading system. In a P2P trading system the list of buyers and sellers might vary at different times of a day, which highly depends on the agents' net energy (energy generated minus energy consumed) and sharing prices, thereby creating a dynamic and complex local market. P2P energy sharing is considered a promising mode for developing the energy market, while the fairness of revenue distribution and utility grid stability is not widely concerned when implementing P2P energy sharing [22]. Recent real-world projects already provide some understanding of the planning, operation, and dynamics of ECs. Notable examples are Brooklyn Microgrid in the USA [23] [24], Quartierstrom in

Switzerland [25] and SonnenCommunity in Germany [26].

The EU introduced the concept of ECs in its legislation in the "Clean Energy Package" adopted in 2019 [15]. ECs have for its primary purpose to provide environmental, economic or social community benefits to its members or shareholders or to the local areas where it operates rather than to generate financial profits. This information is briefly summarised in [27], where one can also find that the EU has launched an Energy Communities Repository [28] and a Rural Energy Community Advisory Hub [29] in April 2022 and June 2022, respectively. The aim of these platforms is to assist local actors and citizens willing to set up an EC through technical and administrative advice, and encourage their development: "Further spread the message of (rural) energy communities to EU policymakers and to citizens across Europe, and thereby raise awareness at the EU level of the cruciality of rural energy communities in the energy transition". The leverage of digital technologies allows a more efficient coordination of the increasingly fluctuating and volatile energy supply in distributed PV systems. Digital coordination mechanisms are key to manage the interaction of electricity supply and demand. Digital technologies such as smart meters are necessary for the measurement of the electricity flows that are provided to the coordination algorithm [20].

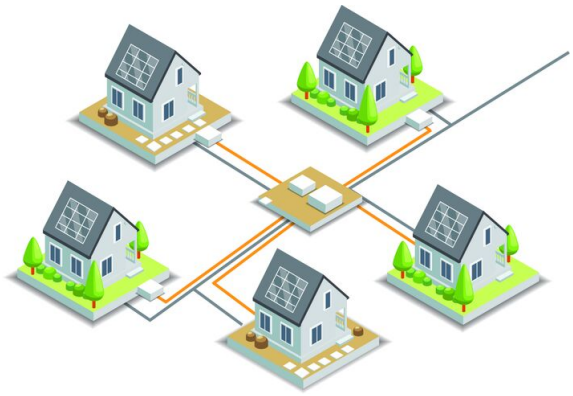

Figure 5: Scheme of an energy sharing system in a neighborhood [30].

1.4.3 Tilt and orientation

Yet another complementary solution to increase self-consumption is by varying the inclination (tilt angle) and orientation (azimuth angle) of the PV system, since the tilt angle of a solar panel can shift production between summer and winter while the azimuth angle shifts production throughout the day. For fixed angles without any solar tracking options there is one angle combination (tilt and azimuth) that maximizes the total energy output of a PV system throughout a year for a specific location [31]. Any deviation from this angle combination will reduce the total output to a certain extent. As a rule of thumb, the output maximizing azimuth is pointing south for the northern hemisphere and the tilt angles are between the latitude of the location (ϕ) and ϕ - 15° with only minor losses in total output (below 5%) in the area of ±15° of the maximizing angle combination [32]. While the output maximizing angle combination is strictly an engineering issue that can be determined for a certain location, it might not represent the maximum value from an energy efficiency or economic perspective. The optimum angle combination depends on the energy and economic values attributed to the self-consumed and surplus PV energy.

Until a few years ago, PV system owners were encouraged to maximize the energy output of their PV systems to compensate with surplus PV energy the times with little or no PV

generation. This was done via high FiTs and wide intervals of time to meter the net energy. However, as self-consumption schemes increase, the question arises whether an output maximizing angle combination, often associated to large amounts of surplus energy, is still preferred over one that enhances self-consumption. For instance, vertical PV facades will produce relatively more power in winter and less in summer, and more in the early and late hours of the day, when the sun is lower in the sky [33].

In reality, the variety of tilts and orientations in a certain building is limited. Moreover, since any deviation from maximum-output angles shifts but reduces the total PV energy output, more PV capacity might be required to achieve reasonable energy outputs, which might also not be possible in an certain building due to a lack of available roof surface. In this sense, an ideal building would have a spherical roof with unlimited surface. An EC may allow for both more roof surface and a wider variety of tilts and orientations, approaching this ideal individual building. This way the EC self-consumption benefits not only from sharing the unavoidable surplus energy by aggregating the load profiles (load consumption aggregation), but also from sharing the different available surfaces and reducing the surplus energy (PV generation aggregation) [34].

1.5 Energy in Norway

As part of its Agreement on the European Economic Area (EEA), Norway participates in the EU's internal energy market and, therefore, cooperates closely with the EU on energy and climate matters [35]. Norway has an agreement with the EU to participate in EU climate legislation for the period 2021-2030 and has committed to reduce emissions by at least 50% and towards 55% by 2030 compared to 1990 levels through its enhanced nationally determined contribution (NDC) under the Paris Agreement [36]. In June 2017, the Norwegian parliament adopted the Climate Change Act, which establishes by law Norway's NDC target as well as the target of becoming a low emissions society by 2050 [37]. In January 2021, Norway's former government presented a white paper to the parliament describing an economy-wide Climate Action Plan for 2021-2030. The main policy instruments in the Climate Action Plan are GHG taxation, regulatory measures, climate-related requirements in public procurement processes, information for the public on climate-friendly options, financial support for the development of new technologies, and initiatives to promote research and innovation [38].

Figure 6 shows an overview of the energy production, supply (production for domestic use) and demand (supply minus losses) in Norway in 2020 by source and sector. Norway's energy demand is highly electrified: in 2020, electricity covered almost half (48%) of the country's total final consumption (TFC), the highest share among IEA member countries, followed by oil (36%), bioenergy and waste (6.8%), natural gas (4.3%), and coal (2.1%). Moreover, Norway has the highest share of RE in TFC among IEA member countries. In 2020, 61% of TFC came from RE, while the IEA average was 13%. Renewables in 2019 provided 90% of TFC in buildings, 71% in industry and 12% in transport. Norway also has the highest shares of RE by sector (industry, transport, buildings) among IEA member countries. At the same time, although fossil fuels accounted for only 52% of Norway's energy supply in 2020, 93% of Norway's domestic energy production consisted of natural gas and oil produced in an environmentally conscious manner. The size of Norway's energy surplus is significant. In 2020, the country produced 10 times more oil and 21 times more natural gas than its domestic needs, with an increasing trend over the past 20 years. Norwegian production of natural gas covers approximately 3% of global demand (third-largest exporter, only behind Russia and Qatar) while Norway's oil production covers about 2% of global oil demand. Russia's 2022 invasion of Ukraine may provide an added incentive for Norway to continue delivering crude to global markets and even increase output wherever possible, since it is

an important contribution to global energy security by serving as a stable and predictable supply [39].

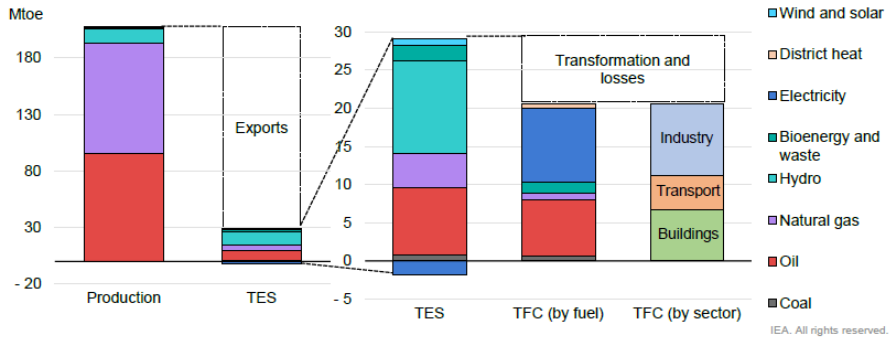

Figure 6: Overview of energy production, supply and demand in Norway, 2020 [39]. TES: Total energy supply. TFC: Total final consumption. 1 Mtoe = 11,63 TWh. Norway exports a large share of the energy it produces, mainly natural gas and oil, as mentioned above. Almost all the electricity generation comes from renewable resources (mainly hydro). Information about the Norwegian's electricity system is given below.

Norway has an almost entirely renewables-based electricity system, with renewable resources accounting for 98% of generation in 2020. In 2020, electricity in Norway was generated mainly from hydro (92%), with some smaller shares of wind (6.5%) and natural gas (1.0%). Other sources include very small shares of bioenergy and waste (0.28%), oil (0.14%), coal (0.03%), and solar (0.02%). Electricity dominates demand in the residential sector (84%), and covers almost half of the energy demand of the industry sector (45%). Together with high and increasing levels of interconnection and integration, Norway provides the Nordic region with a significant source of low-cost, highly flexible, renewable power. Moreover, as electrification forms a central part of any country's energy transition, Norway finds itself in an enviable starting position. Given that nearly all electricity production comes from hydropower and wind power and that Norway is highly electrified, renewables are not currently subject to special treatment or policies, but constitute a central component of the country's domestic energy system. Still, more electrification will be needed across sectors to meet Norwegian climate targets, which will require additional renewable generation capacity, such as continued expansion of hydro capacit, including upgrades of existing plants [39].

Norway's industry and household electricity prices have been the lowest among its neighbouring countries in past years. Nonetheless, the recent surge in electricity prices experienced over winter 2021-2022, led by price spikes in Europe, have raised the issue of vulnerable consumers in the country. In December 2021, the government introduced a temporary support scheme for households with an initial allocation of NOK 8.7 billion until the end of March 2022. When the average spot price over a month exceeded 0.70 NOK/kWh, the government covered 55% of the amount beyond this threshold up to a maximum of 5 000 kWh per month for households. In January, the government increased the coverage rate from 55% to 80%. In March 2022, the support scheme was extended to March 2023, and the coverage rate was raised to 90% for October, November and December 2022. This extension is estimated to cost NOK 7.4 billion [39] [40]. The long-term power analysis published by the Norwegian Water Resources and Energy Directorate (NVE) in October 2021 points to the fact that higher power prices than we have seen historically can be expected in Norway in the future. This is due, among other things, to the fact that the exchange capacity between the Nordics and Europe is increasing and that a persistently high CO2 price is expected in the years ahead. Power prices will increase towards 2030, but fall in

the longer term as RE production in Europe increases [41].

Statnett is responsible for system operation and operational security as well as for developing measures to deal with highly strained supply situations. These are known as "SAKS measures", and their purpose is to reduce the likelihood of rationing. In its analysis for 2021-2026, Statnett assumes that Norwegian power system adequacy, although strained at times, poses no risk of power rationing in the next five years. Through legislation, however, Statnett is given an extended responsibility to continuously investigate and develop necessary measures to ensure that supply and demand are balanced at all times, especially during the winter season. Statnett is preparing changes to its operational model (Nordic Balancing Model), also with the aim to prepare for expected greater shares of variable renewables on the grid. In response, it has developed a plan of grid investments across the country of up to NOK 100 billion by 2030 to handle the increased capacity with a 420 kV grid nationwide. While flexibility in the national power system has historically been provided by abundant dispatchable hydro generation, increased consumption in some important areas (including the Oslo area) reduces the availability of this flexibility source. In the future, flexibility will have to come from the demand side to ensure system balancing. Finally, it must be stressed that Norway is the only country in the world where an advanced metering infrastructure for hourly meter readings has been installed in all households and other measurement points [39].

1.5.1 PV in Norway

Commensurate with the precipitous drop in the cost of installed PV systems, increasing electricity costs and climate concerns, solar systems are proliferating across northern regions, where minimal irradiance and persistent snowfall in winter have traditionally inhibited solar deployment. However, Nordic PV installations benefit from lower temperatures, a large amount of reflected sunlight on the ground (albedo) due to snow and long periods of sunlight in Summer, all of which enhance PV performance. Only PV systems with diverse orientations, such as in ECs or equipped with solar tracking options, benefit fully from the latter, since with fixed installations the Sun at times can be behind the PV modules. The large amount of reflected light due to snow is further enhanced by the use of bifacial modules in field applications, which are characterized by their ability to generate electricity from both sides. The rapid growth of the bifacial PV market can be explained by the relatively low cost of bifacial modules and their perceived advantages. Nowhere are those advantages more apparent than in northern regions where snow may persist on the ground for months. Another advantage of bifacial modules is that the backside does not get covered by snow, so it is possible to produce even when the front side is shaded by snow. PV growth in northern regions is expected to continue at a high rate. This anticipated growth has put pressure on the solar industry to reduce snow shading and increase solar performance in winter. To support those objectives, research is needed in five primary areas related to snow soiling and PV performance: energy losses, performance modelling, system and component reliability, design optimization, and operation and maintenance best practices [42].

Solar PV has been increasing in Norway, but does not form a significant share of the renewable electricity generation mix yet. A more detailed assessment of the competitiveness of solar power without subsidies in the Norwegian context would help to clarify the role that solar can play [39]. It is estimated that 45 MW of PV capacity was installed in 2021, while the total PV generation capacity installed before 2021 was approximately 160 MW. The moderate installation volume is due to a combination of very season dependent solar resources in northern Europe, relatively low electricity prices in the summer season, and moderate financial support. Norway has no defined goals when it comes to implementation of PV technology, although direct support policies for PV installations exist. The public agency Enova SF subsidized, until January 2022, up to 35% of the installation costs for

grid connected residential PV systems at a rate of 7500 NOK per installation and 1250 NOK per installed kW rated capacity up to 15 kW. In early February 2022, these support levels were increased to 2000 NOK per installed kW up to a maximum of 20 kW which will positively impact the outlook for PV installations [43].

The Norwegian government projects electricity demand to grow to 159 TWh in 2030 and 174 TWh in 2040, while generation will grow to 166 TWh in 2030 and 184 TWh in 2040, following Figure 7. The NVE expects that part of the growth in generation will come from new hydro capacity, some of which is already under construction, as well as refurbishments and upgrades to the country's ageing fleet of existing hydro plants. While wind power will see very modest growth through 2025 based on licences already issued, solar PV is expected to see strong growth. The NVE expects offshore wind to only begin to make contributions after 2030. Indeed, on 11 May 2022, the government presented a large-scale plan for offshore wind, with a target of allocating areas for 30 GW of offshore wind capacity by 2040. This corresponds to almost as much power generation capacity as in Norway today [39].

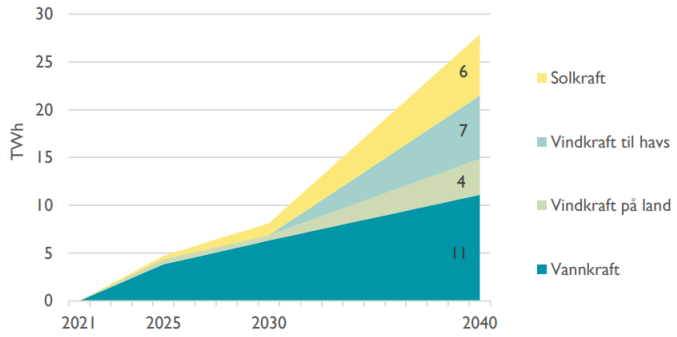

Figure 7: Increase in electricity production in Norway 2021-2040 [41]. The future renewable electricity generation mix is expected to be made up primarily of hydro, wind and solar power. Yellow: Solar (PV) | Light blue: Off-shore wind | Green: On-shore wind | Darker blue: Hydro.

With Norwegian climatic conditions and electricity generation costs, it is not foreseen that large-scale PV plants connected to the transmission grid can be economically feasible. In Norway, PV systems are predominantly installed on residential and commercial buildings. There are already many examples of municipalities that have included PV as a part of the energy system in public buildings. Some municipalities, including the capital Oslo, are establishing policies for increasing PV installations in new and existing public buildings. The transition from fossil fuels to electric energy in the transportation sector increases the domestic demand for electricity. Long term this may indirectly stimulate PV investments [44]. The Norwegian PV market is expected to continue its growth, but it is limited by the fact that use of PV in practice is limited to (individual) self-consumption. If the concept of self-consumption could be extended to consumption in neighbourhoods (allowing energy sharing), the growth rate may increase [43].

2 Literature on PV energy communities

A good review of social arrangements, technical designs and impacts of ECs, not only PV ECs, is made by Gjorgievski et al. [21]. Here, four technology clusters are distinguished in the existing literature: shared solar PV systems, community-owned storage, hybrid energy systems and district heating and cooling. The design objectives are either economic, technical, environmental or social. This report focuses on a technical analysis of a PV EC, so the literature mentioned below has been selected accordingly.

Most of the scientific literature that focuses on local PV energy sharing use either game theory modelling (e.g. cooperative games, non-cooperative games and agent-based) or system analysis modelling (e.g. mixed-integer linear programming). The game theoretical approach has a strong practical relevance due to the modelling of detailed interrelations between agents, whereas system analysis provides a global view on the specified problem. A second classification can be done sorting the publications by the scope of the analysis made. Here, the literature is mainly divided into energy sharing models and profit distribution models (P2P energy trading market), mostly covered by game theoretical models, and sizing models, mostly covered by system analysis modelling. The existing P2P trading approaches can be generally adopted to two scenarios: decentralized P2P market, which involve decision-making participants, and centralized P2P market, where participants are not decision-makers and a market coordinator manages the EC coordination. Numerous P2P trading models arise due to different degrees of effectiveness and fairness of the trading mechanism, potential applicability in real cases and confidentiality of the participants' preferences. An increasing complexity of the EC market structure and decision-making strategies is clearly observed in the research community.

Double-auction mechanisms wherein buyers of energy submit 'ask' prices and sellers submit 'bid' prices, are typically of most interest in decentralized P2P market models. He and Zhang [45] propose a double-auction bidding mechanism that captures the interaction within a community energy sharing market consisting of distributed solar power prosumers and consumers. To determine the double-side auction market spot price, a non-cooperative game is formulated among all participants involved in the community sharing. An iterative algorithm is first designed to clear the market and mitigate the uncertainty in supply and demand. Then, an adaptive pricing strategy is designed to assist agents better estimate the market and predict the future price. Li and Ma [46] propose, using non-cooperative game modelling, a bidding-based double-auction P2P electricity trading system that enables to fairly distribute total profits obtained from P2P trading to each community house, and with no need of complex trading strategies and learning abilities. Using an agent-based model, Nuñez-Jimenez et al. [47] simulated the decision-making of nearly 5000 building owners in a city district in Zurich, Switzerland, and assessed three locally relevant policy scenarios: no community solar, community solar with adjacent buildings, and community solar with buildings within a 100-meter radius. The findings demonstrate the potential of community solar to accelerate PV adoption in cities and underscore the significant role of policy design in achieving this goal.

Wang et al. [48] propose a centralized P2P energy trading model for residential households, and the objective is to help the centralized market coordinator optimize the benefit of participants under such a P2P market. To this end, a new mathematical model, including the rules for buying and selling energy, is presented. In this model, a supply function bidding mechanism is formulated to match the power supply imbalance and calculate the market-clearing price. An optimization problem is formulated to identify the optimal strategies for energy buying and selling, which consists of two parts: the first part is to maximize the social welfare; the second part is to minimize the unfair benefit distribution that partici-

pants can gain through P2P energy trading. Henni et al. [20] find questionable whether inexperienced participants would understand the consequences of their participation and their actions in an energy trading mechanism, even if the decisions are made by an intelligent agent in a centralized P2P market. They propose an "agreed cost-sharing mechanism" based on a fixed pricing approach to achieve a fair distribution of the profits generated through the sharing economy. They further investigate the impact of prosumers' and consumers' load profile patterns on the profitability of the sharing communities. Based on these findings, they explore the potential to match and coordinate suitable communities through a platform-based sharing economy model. Finally, they show that the selection of suitable participants, based on load profile properties, can enhance the potential revenues and also the incentive to participate in sharing local electricity. Zhao et al. [22] propose an innovative energy management method integrating P2P energy sharing with demand-side management (DSM), to achieve fair revenue distribution and stable interaction between the community microgrid and the utility grid. Generally, residential electricity load can be categorized into two types, i.e., basic load and flexible load. Flexible load refers to electrical load with adjustable operating time or power without affecting the comfort of the occupant, which is the basis for implementing DSM. An energy sharing coordinator acts as the operator of the community and is in charge of establishing a uniform pricing and energy allocation mechanism based on the ratio of supply to demand. Ali et al. [49] propose a peer-to-grid (P2G) energy trading combined with peer-to-peer (P2P) energy trading scheme based on a cooperative game theoretical technique to optimize sizes of the generation resources and battery, and achieve maximum payoff from a networked microgrid. The selected architecture consists of two microgrids in which both microgrids contain not only solar panels, but also wind turbines and batteries to meet the requirements of the load.

Xu et al. [50] integrate a residential PV panels planning model with the energy sharing mechanism. In their proposed model, all prosumer agents form a coalition to maximize cooperatively their common benefits by operating their residential PV panels. They implement a novel two-stage game-theoretic framework of residential PV panels planning. In the first stage, Stackelberg game theory is used to model the stochastic bi-level energy sharing problem, which is solved by their own algorithm based solution method, so the optimal installation capacity of residential PV panels can be obtained with uncertain PV energy output, load demand, and electricity price. In the second stage, we develop a stochastic programming-based optimal power flow model to optimally allocate residential PV panels for all PV prosumers with minimum expected active power loss. Similarly, Yang et al. [51] propose a novel two-stage optimization model of design and electricity dispatch strategies for residential PV communities to operate electric vehicles' charges. The first-stage optimization aims to obtain the optimal capacities of PV and batteries. The second-stage optimization optimizes the retailer's hourly electricity prices and electricity dispatch strategies, in which the Stackelberg game is performed between maximizing the retailer's benefit and minimizing the electricity cost of residential basic loads and vehicle charging loads.

Some publications disregard the trading business modelling and focus purely on the energy sharing from a more electrically operative point of view. Lorenzo et al. [52] propose an innovative system architecture based on a common dc bus that is used to deliver the energy produced by the generator to different consumers, with the presence of a balance node used to feed into the grid the in excess produced power. The system architecture supports only a unidirectional power flow from the common generators to the users, avoiding any exchange of power among the users and preventing them from supplying power into the grid, thus complying with any regulation framework. Hutty et al. [19] consider the possible advantages of a P2P energy market to complement PV generation and EVs, in the setting of a community of households forming a grid-connected microgrid. The results show that P2P is a very interesting innovation that could greatly assist the integration of a high penetration

of PV and EVs in the built environment. It can enable significant gains in energy independence (which should correspond to a reduction in emissions) and significant reduction of household bills, especially when PV penetration is high. Zabihinia Gerdroodbari et al. [53] use peer-to-peer data to propose a novel reactive power-based control strategy for single-phase PV inverters to simultaneously improve voltage unbalance and voltage regulation in low-voltage distribution networks.

Some publications disregard the interrelations between the agents within the EC and aim to analyze the EC from a holistic approach, typically using system analysis modelling. This is the approach targeted in this report. A good overview of the existing literature concerning system analysis modelling is done by Mehta and Tiefenbeck [54]. Although the focus is on individual PV generation and battery storage, Li [55] also investigates group battery optimizations for communities with different consumption levels or with different energy demand diversity to see their effects on optimal sizing and peak demands for aggregated PV-battery system. The optimization does not only generate optimal battery and PV size but also provides corresponding battery charge/discharge operations under a time-of-use electricity tariff. Although individual optimal batteries can significantly reduce energy cost, a group battery offers more value for cost saving, especially for groups with sufficient diversity in their demand profiles. Fina et al. [56] analyze the profitability of shared, non-subsidized PV systems' usage in fictitious multi-apartment buildings in Austria. It compares the Austrian results with those of Germany, where significantly higher retail electricity prices determine the profitability benchmark. To that end, a multi-objective optimization model is developed for the optimal dimensioning of PV systems and energy storage facilities in keeping with different end user objectives, ranging from minimizing annual electricity costs to maximizing self-consumption. The results of this paper show that the economic viability of shared PV systems strongly depends on the absolute value of the variable component of the retail electricity price. For Germany, a country with a high retail electricity price (due to high renewable energy surcharges), the concept is clearly profitable, whereas economic viability is nonexistent or marginal in Austria. In Austria, no profitability is observed in case of matching PV generation and loads for individual apartments, and a small cost-saving potential is found in the case of aggregation of all apartments' loads.

Heinisch et al. [57] develop and optimization model that minimizes the annual costs, including investment costs, to investigate and compare the costs incurred by individual households and households organized in electricity trading communities in seeking to attain greater independence from the centralized electricity system. This independence is investigated with respect to: (i) the potential to reduce the electricity transfer capacity to and from the centralized system (increasing self-consumption) and (ii) the potential to increase self-sufficiency. Utilizing measured electricity demand data for Swedish households, they show that with a reduced electricity transfer capacity to the centralized system, already a community of five residential prosumers can supply the household demand at lower cost than can prosumers acting individually. Grouping of residential prosumers in an electricity trading community confers greater benefits under conditions with a reduced electricity transfer capacity than when the goal is to become electricity self-sufficient.

The optimal PV/BESS sizing in the P2P trading was performed by Yaldız et al. [58] by maximizing the return of PV and BESS to the users and the net profit after deducting their costs. Users benefit from optimal PV and BESS sizing in terms of both social welfare and economic profit. Capital, replacement and maintenance costs were taken into account for precise sizing. Furthermore, the economic contribution of P2G and P2P energy exchange situations were examined. The use of P2P energy trading has resulted in substantial benefits for both prosumers and customers in the proposed scheme.

Radl et al. [13] analyze different community configurations on costs and investments considering country specific conditions. Results show that renewable energy communities have the potential to reduce electricity costs due to community investments and load aggregation but do not necessarily lead to more distributed PV. Besides full-load hours, the energy component of electricity tariffs has the highest impact on PV distribution. Self-consumption oriented PV systems need high procurement prices to be competitive. Under current market conditions, battery energy storage systems are rarely profitable for increasing PV self-consumption but there is potential with power pricing.

Fina et al. [59] investigate the profitability and optimal installation capacities of PV systems for energy communities (ECs) in comparison to individual buildings. To gain a wide spectrum of results, four characteristic settlement patterns with different building types are defined, ranging from urban to suburban and historical to rural areas. Analytically, a MILP model is developed to maximise the net present value (NPV). The results show that the profitability of implementing optimally-sized PV systems increases when forming ECs compared to the situation of considering buildings individually. Forming an EC is most valuable for SFHs in rural areas, which can then profit from synergy effects between different load profiles. Generally, PV system implementation is most profitable the more heterogenous load profiles are considered. Participants providing large roof/facade areas can significantly contribute to increasing the cost saving potential for the whole community. This aspect is highly important when considering that some buildings might not have the possibility of installing PV. Battery- and hot water storage which complement PV systems and heat pumps can contribute to saving energy costs, if only marginally.

Freitas et al. [34] explore the combined effect of aggregating building demand, photovoltaic generation and storage on the self-consumption of PV and its impact on the grid. In particular, its main goal is to evaluate to what extent the building integration of PV alone avoids costs of extra storage while remaining profitable for users and innocuous for the grid. The methodology considered that the PV systems placement is optimized using a genetic algorithm for maximization of self sufficiency and minimization of net load variance on the electricity grid, as well as a storage strategy for self-consumption maximization and another for the minimization of net load variance. Findings confirm that the multitude of building surfaces with different tilts and orientations in the urban environment translates into a great PV potential that, if well used, results in a better demand–supply match. When the placement of the PV systems is optimized by tilt and orientation, the aggregation of the demand from different buildings and the PV systems improve that relationship, minimizing storage needs. The results also show that, from the point of view of prosumers, investments on PV may be viable with no or very small added storage capacity. But from the electricity grid point of view, unmanageable net load variance and consequent costs could be mitigated through higher storage capacities with proper management strategy.

Proper energy storage system design is important for performance improvements in solar power shared building communities. Existing studies have developed various design methods for sizing the distributed batteries and shared batteries. The effect of storage is strongly influenced by its sizing and operating strategy. Some of the publications mentioned below consider energy storage in their system modeling. Huang et al. [60] integrate the considerations of aggregated energy needs, local PV power sharing, advanced community control, and battery storage sharing, which will be useful to optimize three functions (energy efficiency, energy production and flexibility) in a positive energy district towards energy surplus and climate neutrality.

This report focuses on a technical analysis, and hence disregards any economic, environmental or social impacts that ECs may entail. Economic and environmental assessments are

well covered in the existing literature, including some of the publications mentioned above, but social concerns in ECs are very rarely investigated, so a couple of relevant publications are mentioned next. Soeiro and Dias [61] collect data, using a survey on European countries, to study and to better understand what the citizen energy initiatives are, their main features and the motivations of individuals to participate on it. The citizens participation is a crucial point for the development of this type of communities. The main motivation for participation in these communities seems to be concerns about environmental and climate impacts. They find that the reason "lower energy costs" and "local income generation", which was forecasted as a relevant motivator, seems to be pointed out by the participants as one of the least important factor. It is clear that citizen recognize that ECs add non-monetary values to the communities in which they operate. Among these values are the promotion of energy transition, energy guidance, and social and green action activities. Drawing on data collected among 71 European RECs, Hanke et al. [62] investigate on the high expectations set on RECs to become democratic, transformative and equity-enhancing actors for a just transition. While some are interested in engaging in or already engage in energy justice, others do not resonate with the energy justice concept. Consequently, referring to RECs as equity-enhancing actors of a just transition and contributing to energy justice must be done more carefully than is currently the case. Ideally, national legislation would link enabling conditions for RECs to the requirement to engage in a social role. In consequence, RECs would gain an advantage when engaging in activities linked to energy justice.

3 Motivation and objectives

3.1 Motivation

In light of the expected high PV penetration to fight climate change and the increasing electricity prices, energy communities (ECs) have become a promising topic withing the energy field [1] [21]. A PV EC allow prosumers to share self-generated PV energy, increasing self-consumption and energy efficiency compared to having PV on individual buildings with no energy sharing. This is done via load aggregation, PV generation aggregation and potential battery storage aggregation.

An increased self-consumption has three main consequences: improved grid stability, reduced carbon emissions and potential cost savings. By increasing the self-consumption, there is less surplus energy fed-back to the grid (at peak generation times), preventing grid operators from facing technical challenges associated with voltage and frequency violations or line overloads, which entail extra reinforcement grid costs [18]. A higher self-consumption may lead to less energy taken from the grid as well, which is typically generated using polluting resources, such as fossil fuels. In this sense, ECs can help reduce carbon emissions and mitigate the impacts of climate change [63]. A higher self-consumption may translate into energy economic savings as well. Nonetheless, multiple variables play an important role here, such as the distribution of profits, the value of electricity/grid costs (variable and fixed) and the value given to the surplus PV energy (FiTs). Saving costs could be associated with savings on the PV initial investment too, if the EC benefits from economies of scale or if the increase in self-consumption allows for a lower installed PV capacity [13]. Some other advantages can be found, such as community building. By coming together to form a PV EC, members can build stronger social connections and foster a sense of community around RE, which may promote the use of RE in society and raise awareness about the importance of sustainability and environmental protection [61].

Many authors investigate possible operating models as well as the financial benefits of sharing PV generation in ECs, but often disregarding the PV sizing optimization problem. In February 2018, a multi-objective optimization model, focused on minimal annual electricity costs and maximal self-consumption rate, is developed by Fina et al. [56] for the optimal dimensioning of PV systems, but it focuses on P2P trading only in multi-apartment buildings. In September 2020, Xu et al. [50] include a PV planning in their model using a Stackelberg game, and state: "Different from most works related to residential PV panels planning, we innovatively integrate a residential PV panels planning model with the energy sharing mechanism. To our best acknowledge, this has not been studied before. In this way, we can improve economic benefits to PV prosumers and meanwhile facilitate the installation of residential PV panels, which has practical significance." In September 2021, Yaldız et al. [58] develop an optimal PV/battery sizing model in a P2P context using a MILP-based algorithm structure and state: "Optimal sizing in renewable energy and energy storage systems in distributed grid systems was studied extensively. However, the existing studies on optimal PVs and BESS sizing in the P2P energy market were limited". Yaldız et al. [58] mention the publication by Ali et al. [49], which optimizes sizes of different coupled generation resources (PV and wind turbines) based on a cooperative game theoretical technique, as the only one considering PV sizing under a P2P context. The objective of the sizing models in the three last mentioned publications above is maximizing the economic profit.

An EC may allow for both more roof surface and a wider variety of tilts and orientations. Sharing the multiple roof surfaces in the EC can produce varying levels of energy at different times of the day and year, potentially increasing the EC self-consumption. This is something very rarely investigated by the research community when tackling the PV/battery sizing optimization problem in an EC. This is addressed as future work by Awad and

Gül [64]. Yang et al. [51] take into account the tilt of the PV modules in the first-stage of their optimization model, which aims to obtain the optimal capacities of PV and batteries minimizing investment cost. However, just one single possible tilt angle is considered. Fina et al. [59] consider different orientations (south, east, north and west) and tilts (30° roofs and 90° façades) in different EC different settlement patterns using a MILP optimization model. However, the only objective is economic maximization. Freitas et al. [34] consider the multiple orientations and tilts in two different ECs, concluding that a multitude of building surfaces with different tilts and orientations in the urban environment translates into a great PV potential that, if well used, results in a better demand–supply match. When the placement of the PV systems is optimized by tilt and orientation, the aggregation of the demand from different buildings and the PV systems improve that relationship, minimizing storage needs.

3.2 Objectives

In general, just a few publications address the PV sizing problem in an EC context, which introduces new challenges compared to installing PV on individual buildings due to the existence of multiple orientations and tilts, which are somehow shared by the EC members in terms of PV generation, and due to the existence of multiple load consumption profiles. Taking full advantage of the available surfaces can improve the overall energy efficiency of the EC by matching more accurately the PV generation to the load consumption profile. The aim of this report is to provide technical advice to facilitate the decision-making regarding the PV installation in a residential PV EC. A sizing optimization model is developed and applied to an upcoming residential PV EC formed by 100 households in Harstad, Norway [2]. A projected view of this EC is observed in Figure 8.

Figure 8: Upcoming residential PV EC formed by 100 households in northern Norway (Harstad, 68°N 16°E) [2].

Different tilts and orientations are considered in the model, as well as a battery storage with different sizes, to find optimal system sizings that fit to different energy goals. To this end, three softwares are used, as described by Figure 9: System Advisor Model (SAM), Load Profile Generator and Microsoft Excel. SAM is used to calculate PV generated energy for different orientations and tilt combinations. Load Profile Generator is used to generate multiple load consumption profiles. The data obtained from these two softwares is inputted in Excel. Excel is used to define and solve the sizing optimization problem. The Excel solver "GRG Nonlinear with multistart" is used to find the optimal PV capacities for certain battery capacity sizes and energy goals based on self-consumption metrics, such as the self-consumption rate (SCR), the self-sufficiency rate (SSR) and the energy balance index (EBI).

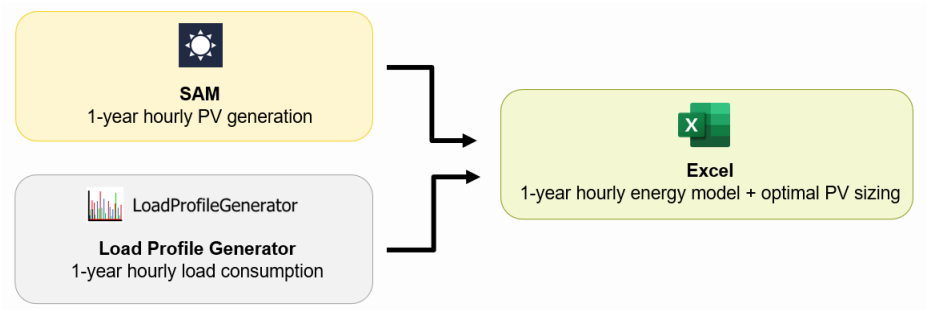

Figure 9: Scheme of the methodology followed.

The model developed in Excel is validated in terms of inflows and outflows of energy (to/from battery, to/from load, to/from grid) by comparing the model results with results from SAM, for arbitrary installed PV/battery capacities in the specific location. The optimal PV capacities solutions provided by the "GRG Nonlinear with multistart" Excel solver are validated by solving the optimization problem with another Excel solver, the "Evolutionary" solver, which uses a totally different solving algorithm than "GRG Nonlinear".

Before presenting in detail the methodology followed and the results, relevant theoretical concepts are explained in the next chapter.

4 Theory

4.1 Configuration of a PV system

The different components of a grid-connected residential PV system are shown in Figure 10. The PV panels (or modules) transform a certain amount of the solar energy into DC electricity, which is then converted into "useable" AC electricity by means of an inverter. To maximize the power output from the PV modules, a maximum power point tracker (MPPT) has to be used, which may or may not be integrated on the inverter, depending on the layout. Some of this converted electricity is utilized to power the loads, either directly or by means of a battery storage, while the excess is fed-back into the utility grid. A meter is installed to account how much excess energy is fed-back into the grid and how much energy is taken from the grid. There are two main system layouts for residential PV systems with battery storage; either AC coupled where the battery is connected via an inverter and a charge regulator (controller) to the AC link of the PV system (scheme on the left), or DC coupled where the batteries are connected to the DC link of the inverter (scheme on the right) [17].

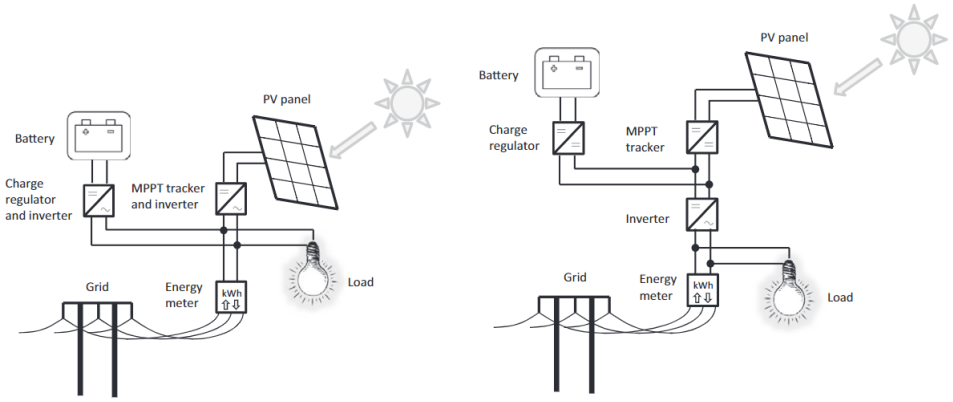

Figure 10: Simplified system layouts of AC coupled (left) and DC coupled (right) grid-connected residential PV/battery systems [17].

4.2 Solar irradiance

The main angles that are relevant when determining the solar radiation on a solar module or array are shown in Figure 11. The tilt (β) and orientation (γ) of the module only depend on the position of the module, which is typically fixed. The solar zenith angle (θ_z), the solar altitude angle (α_s) and the solar azimuth angle (γ_s) only depend on the position of the Sun, which varies with location and time. The incident angle (θ) depends on both the position of the modules and the position of the Sun, so this angle changes with location and time as well.

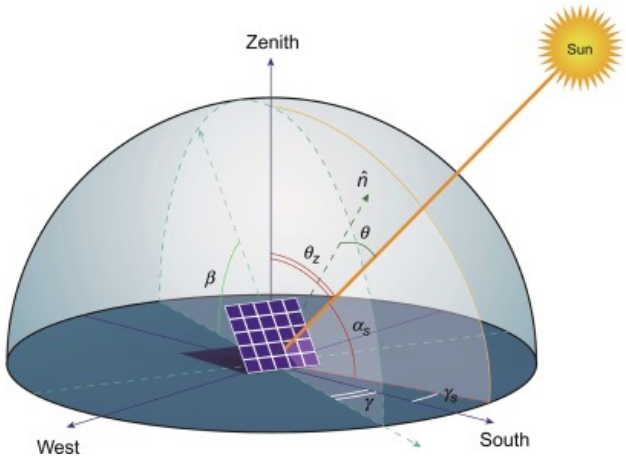

Figure 11: Key angles to determine the solar radiation [65].

The most relevant angle is the angle of incidence (θ), which is given by Equation 1:

$$cos(\theta) = cos(\beta)cos(\theta_z) + sin(\beta)sin(\theta_z)cos(\gamma_s - \gamma) \tag{1}$$

The total solar irradiance on a horizontal plane (GHI), as if the modules were placed flat on the floor, can be calculated as the sum of a direct-beam radiation and a diffuse radiation (Equation 2).

$$GHI = DNI \times cos(\theta_z) + DHI \tag{2}$$

where DNI is the direct normal irradiance (irradiance on a perpendicular plane to the sun rays) and DHI is the diffuse horizontal irradiance (irradiance scattered by the earth's atmosphere). Typically, GHI, DNI and DHI can be found from historical measurements in weather stations or from satellite data.

The total solar irradiance on the plane of array (G_{poa}), understanding plane of array as the plane where the modules are placed (considering the tilt and the orientation), is calculated transposing GHI into the plane of array. The G_{poa} can be calculated as the sum of a direct-beam radiation, a diffuse radiation and a ground-reflected (albedo) radiation, as Figure 12 shows.

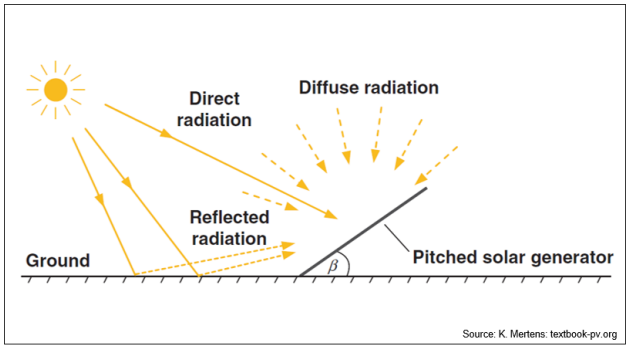

Figure 12: Components of the solar radiation for a tilted module: direct-beam, diffuse and ground-reflected radiation.

The direct-beam radiation is dependent on DNI and θ.

The diffuse radiation can be calculated in different ways, all of which depend on at least DHI and β. The simplest way is by assuming that the diffuse radiation is uniformly distributed across the sky, following the Isotropic model [66]. In this model a 'sky view factor' accounts for the diffuse radiation: $(1 + cos\beta)/2$. This view factor ranges from 0.5 (β=90°, vertical panel) to 1 (β=0°, flat panel). More complex and accurate transposition models exist that account for the diffuse radiation differently. The HDKR model also assumes isotropic diffuse radiation, but accounts for the higher intensity of circumsolar diffuse radiation, which is the diffuse radiation in the area around the Sun [67]. The Perez model uses a more complex computational method than the other two methods [68]. This model differs from the Isotropic and HDKR models in that it uses empirical coefficients derived from measurements over a range of sky conditions and locations instead of mathematical representations of the sky diffuse components. It accounts for both isotropic and circumsolar diffuse radiation, as well as horizon brightening [69].

The ground-reflected radiation, which can indeed be considered as a form of isotropic diffuse radiation, is dependent on GHI, the albedo coefficient (ρ_g), ranging between 0 and 1, and a second 'sky view factor': $(1 - cos\beta)/2$. This view factor ranges from 0 (β=0°, flat panel) to 0.5 (β=90°, vertical panel).

The overall transposition equation according to the Isotropic model is given by Equation 3. It can be pointed out that only the direct-beam radiation depends on θ. Indeed, if β=0° (flat module) Equation 3 becomes Equation 2 since $\theta = \theta_z$ if β=0°.

$$G_{poa} = DNI \times cos(\theta) + DHI \times \frac{1 + cos(\beta)}{2} + GHI * \rho_g \times \frac{1 - cos(\beta)}{2} \tag{3}$$

4.3 PV performance

When manufactured, each module is tested under standard test conditions (STC) to determine its performance characteristics. STC involve testing the module under an irradiance of $G_{STC} = 1000W/m^2$ with an incident light spectrum corresponding to an Air Mass value of 1.5, both conditions together referred to as the AM1.5G spectrum. The G stands for global and includes both direct and diffuse radiation. The test requires that the temperature of the module remains at $T_{STC} = 25°C$. The Air Mass (AM) is the path length which light takes through the atmosphere before striking the Earth's surface, normalized to the shortest possible path length; that is, when the sun is directly overhead (see Figure 33 in Appendix). The AM quantifies the reduction in the power of light as it passes through the atmosphere and is absorbed by air and dust. It is directly related to the solar zenith angle (θ_z) and solar altitude angle (α_s) through $AM = 1/cos(\theta_z) = 1/sin(\alpha_s)$, so AM=1.5 corresponds to $\theta_z = 48.2°$ or equally $\alpha_s = 41.8°$. These standard testing conditions are chosen because they represent the average conditions that occur at the Earth's surface on a clear day at noon. Six main parameters are measured under these STC conditions to determine the module's performance, which are typically given in the module data sheet specifications: open-circuit voltage (V_{oc}^{STC}), short-circuit current (I_{sc}^{STC}), maximum-point voltage (V_{mp}^{STC}), maximum-point current (I_{mp}^{STC}), maximum-point power (P_{mp}^{STC}) and the efficiency (η). The first five parameters are shown in Figure 13.

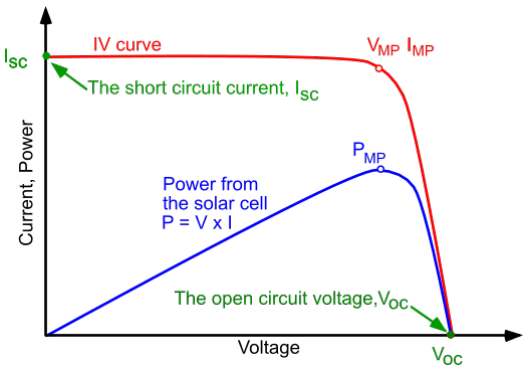

Figure 13: I-V and P-V curve of a random PV module amd key parametres [70].

As shown, the power is the voltage times the current, so P_{mp}=V_{mp}*I_{mp}. The units of power are W ($Watts$) but when the STC maximum-point power (P_{mp}^{STC}) is considered the units are typically Wp, where p stands for peak. The STC efficiency of the module (η^{STC}) is then calculated by the ratio between the maximum output power density of the module (P_{mp}^{STC}/A) and the input solar irradiance (G_{STC}), following Equation 4.

$$\eta_{STC} = \frac{P_{mp}^{STC}}{G_{STC}A} \tag{4}$$

where A is the area of the module.

As mentioned above, these parameters appearing on the module's datasheet are measured under STC conditions, but a PV module is exposed to changing temperature and solar irradiance conditions during operation, which makes the the values of voltage and current vary, changing the output power P_{mp}.

In terms of temperature dependency, the voltage decreases significantly (linearly) with increasing temperature whereas the current barely increases (linearly) with increasing temperature. The power is the voltage times the current so it basically decreases with increasing temperature. A simple way to account for the temperature dependencies is by considering the temperature coefficients provided by the manufacturer in the module's datasheet, following Equations 5, 6 and 7. These temperature coefficients are typically $\alpha = 0.05\%/°C$, $\beta = -0.3\%/°C$ and $\gamma = -0.4\%/°C$.

$$I(T_{mod}) = I_{STC}(1 + \alpha(T_{mod} - T_{STC})) \tag{5}$$

$$V(T_{mod}) = V_{STC}(1 + \beta(T_{mod} - T_{STC})) \tag{6}$$

$$P(T_{mod}) = P_{STC}(1 + \gamma(T_{mod} - T_{STC})) \tag{7}$$

where T_{mod} is the temperature of the module. Some models exist to determine the module's temperature during operation, such as the NOCT model [71], the Heat transfer model [72] or the Sandia temperature model [73], which are based on parameters like the plane-of-array irradiance (G_{poa}), the air temperature, the wind speed, the transmittance-absorbtance product, some parameters given by the module's mounting configuration or some specifications given in the module's datasheet [69].

In terms of solar irradiance dependency, the voltage barely increases (logarithmically) with increasing irradiance whereas the current increases significantly (linearly) with increasing

irradiance. The power is the voltage times the current, so it basically increases (linearly) with increasing irradiance. The module's efficiency, which describes ultimately the performance of a module, maintains a strong dependency with temperature, based on how the power decreases significantly with increasing temperature and is barely influenced by irradiance, since a change in the irradiance affects evenly the input and output power densities (numerator and denominator) in the efficiency expression.

However, several assumptions lie behind this way of addressing the module's dependency with temperature and irradiance, which may be named as the STC module's performance model. The temperature coefficients provided in the datasheet (α, β and γ) lose accuracy if the actual operating conditions deviate significantly from the STC conditions. Moreover, the linear dependency of P_{mp} with irradiance is true as long as the irradiance is not too low (below around $200 W/m^2$). Below this irradiance value, P_{mp} decreases non-linearly with decreasing irradiance, and hence the module's efficiency is no longer uninfluenced by irradiance.

More sophisticated and accurate module's performance models exist, both based on theoretical and empirical approaches. The Sandia model is an example of an empirical model that calculates module voltage and power at five points on the module's I-V curve using data measured from modules and arrays in realistic outdoor operating conditions [73]. The theoretical models are typically based on diode equivalent circuits, more specifically on the well-known Single-diode model described by Soto et al. [71]. The equivalent circuit for this model is shown below in Figure 14.

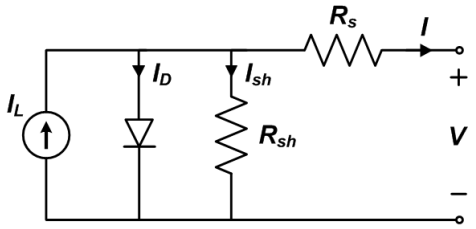

Figure 14: Single-diode model equivalent circuit [74]. I_L: light current. I_D: diode current. I_{sh}: shunt current. R_{sh}: shunt resistance. R_s: series resistance. I: total current. V: applied voltage.

This equivalent circuit is governed by five parameters, as described by Equation 8: the modified diode non-ideality factor a, the light current I_L, the reverse saturation current I_0, the series resistance R_s, and the shunt resistance R_{sh}.

$$I(V) = I_L - I_D - I_{sh} = I_L - I_0 \left[\exp\left(\frac{V + IR_s}{a} \right) - 1 \right] - \frac{V + IR_s}{R_{sh}} \tag{8}$$

These five parameters can be derived at STC from solving Equation 8 at certain I-V points given by the module specifications provided on manufacturer data sheets. Some tools exist that calculate these five parameters at STC, such as the Dobos calculator [75], an algorithm developed for the California Energy Commission (CEC) six-parameter module's performance model, which is based on the five-parameter Single-diode-model. Auxiliary equations, functions of both temperature and irradiance, are used to translate the five parameters at STC into non-STC operating conditions at every time step. Then an iterative solving method (Newton Raphson for instance) finds the voltage and current values that satisfy Equation 8, generating the non-STC IV curve, and extracting the maximum-power point, i.e. P_{mp}=V_{mp}*I_{mp}. Dobos and MacAlpine [76] state that the Single diode model is

a common way to represent the current-voltage (I-V) characteristic of a PV module, and has been extensively documented in the literature as well as deployed in several commercial software models in various forms (PVsyst, SAM, PV*SOL). However, they state as well that the primary reason for the Single diode model's inaccuracies emerges from the choices of the auxiliary equations. They developed a ten-parameter model based on the five-parameter Single diode model that presents an approach to improve prediction accuracy of the Single diode model by leveraging test data collected according to the IEC-61853 standard, for which the module is tested at multiple irradiance and temperature conditions, not only at STC.

These module's performance models take into consideration the light that is being absorbed into the module and effectively converted into electricity, and the light that is being transmitted through the module and lost. This is numerically described by the module's efficiency (η). During operation, the light to be either absorbed or transmitted has to be not reflected. Reflection losses, also known as incidence angle modifier (IAM) losses, are a type of energy loss that occur in PV modules when sunlight hits the surface of the module at an angle of incidence (θ) other than perpendicular. Therefore, angles of incidence different from 0 not only lead to less direct-beam solar radiation in the plane-of-array, as explained in the solar models above (see Equation 3), but also cause more sunlight to reflect away from the module's surface. The amount of reflection losses depends on various factors such as the angle of incidence, the type of module, and the anti-reflective coating (ARC) used on the module's surface. Under STC conditions, the incident light is perpendicular to the module, leading to an angle of incidence equal to 0, so no reflection losses occur. This is why reflection losses are not considered in the STC module's performance model since it is solely based on measurements taken under STC. Some sophisticated module performance models such as the Single diode model or the Sandia model include an angle of incidence assessment to adjust the direct-beam radiation to account for reflection loss.

4.4 PV performance in northern latitudes

In northern latitudes, deviations from STC are more frequent than in lower latitudes, making it necessary to use a module's performance model that accounts for these deviations. These deviations pose both advantages and disadvantages in the PV performance, as explained below.

4.4.1 Snow

Snow has a positive effect on power generation as it increases the ground-reflected radiation (albedo) significantly. While an albedo coefficient of 0.2 is assumed for most of the PV system installed in urban environments [77], the albedo coefficients for fresh new snow, old dirty snow and white ice are, respectively, 0.8-0.9, 0.6-0.7 and 0.4-0.5 [78]. The positive effect increases when the module tilt angle (β) increases, following the third term of Equation 3 [79]. However, snow adhesion to the module surface, also known as snow shading, causes significant energy losses. Snow can persist on solar panels for days to weeks, depending on prevailing climatic conditions and also on the design of the PV array. While more data are needed to quantify losses regionally and globally, snow shading is clearly detrimental to PV performance [42]. Moreover, heavy snow loads can lead to further energy loss by damaging the modules due to its high weight or because of icing [79].

There are two primary mechanisms by which snow sheds from the module surface, melting and sliding, though the two are interrelated. Snow sliding has been reported several times as the most common cause of snow removal [79]. Snow sliding is generally triggered by a reduction in frictional forces, which may occur when a thin layer of melted snow forms at the module surface or when the weight of the snow is sufficient to overcome surface resistance,

causing detachment at the snow-substrate interface. Sliding can occur relatively quickly thereafter, although it may be non-uniform if there is partial shading of the array. Sliding can also occur at ambient-air temperatures below freezing if there is sufficient irradiance for some melting to occur and depending on the tilt angle. Melting typically occurs when the snow layer is thin and able to melt quickly as the air temperature rises to near or above 0°C, a process that is accelerated by high solar irradiance [42].

A key challenge to the deployment of PVs in snow-prevalent areas is predicting accurate annual energy yields for PV systems, given the inherent intra- and inter-seasonal variability of snowfall and the many factors that contribute to snow adhesion to modules. Several attempts have been made to estimate yearly energy losses attributable to snow on PV panels, but the published data reflect a limited number of sites, small study sizes, and incomplete accounting of the variables that contribute to snow losses. Overall, there are at least 11 models to quantify energy losses due to snow. Few comparative studies have been performed. Some have been validated at multiple sites, often in the United States, while others remain relatively untested. There is no consensus as to which model is most accurate and more validation work is needed at different latitudes, tilt angles, and mounting configurations [42].

Snow modelling can be divided into two branches: direct energy loss prediction, consisting of stochastic and curve-fitting methods from historical data, and snow coverage prediction, consisting of threshold-based and first principle methods. In the direct energy loss approach, stochastic methods use only historical PV array output data, whereas curve-fitting methods develop empirical correlations between array output and historical weather data, like in the work made by Awad et al. [80]. By contrast, models that estimate energy losses by predicting the shedding of snow from PV panels are more complicated, like in the work made byMarion et al. [81]. Here, threshold models define physics limits that, if surpassed, result in snow sliding off a module at a defined rate [42]. The Marion model is incorporated into the National Renewable Energy Laboratory's (NREL) System Advisor Model (SAM), which is the PV software used in this report [82] [69].

4.4.2 Other aspects

High latitude sites often experience prolonged periods of weak or no sunlight during the winter due to low solar altitudes. In addition, these low solar altitudes may lead to high angles of incidence, depending on the position (orientation and tilt) of the module, causing relatively large reflection losses. These two facts, especially the former one, decrease considerably the sunlight absorbed by the PV module. Low irradiances decrease the module's output power (P_mp) not only because the trivial fact that less sunlight hits the surface, but also because, as explained before, for irradiances below around 200 W/m^2, very frequently observed in a Nordic site, the linear relationship between power output and irradiance breaks down. Therefore, the module's efficiency (η), which remains roughly constant and equal to the STC value with irradiance values above 200 W/m^2, is reduced. Nevertheless, the combined winter reductions due to angle of incidence and low light are generally only 3% or 4% of annual energy production because of the so much higher summer insolation. This higher summer insolation is due to higher altitude angles and a larger solar azimuth range compared to to winter months, resulting in long periods of sunlight, not observed in lower latitudes. With fixed installations not all the direct insolation can be utilized, since the sun at times can be behind the module [42]. This is why PV systems with solar trackers or diverse orientations/tilts, the latter potentially observed in ECs due to the variety of houses, can make the most of this large range of the solar altitude and azimuth angles and produce PV energy throughout the entire day and year.

Moreover, a cold climate is favourable for the PV performance, since it has been already

mentioned that the efficiency of a PV module is enhanced by low temperatures. Finally, frequent precipitation helps to avoid soiling of the modules, which is another energy loss not mentioned so far that is especially detrimental in arid regions [83].

4.5 PV system analysis

The raise of prosumers, self-consumption trends and energy sharing mechanisms have changed the way of designing and evaluating a PV system. Luthander et al. [17] identified in 2015 key technical indicators when self-consumption is aimed, as well as important factors affecting self-consumption metrics. It could be stated that it was in 2015 when self-consumption started to be of interest in the research community. Gjorgievski et al. [21] identified in 2021 the indicators used to quantify the economic, environmental, technical and social impacts of EC projects. It can be observed that the two main technical metrics used by the researchers are the self-consumption rate (SCR) and the self-sufficiency rate (SSR), while the main economic metrics are the energy bill savings and the total cost savings. Although SCR and SSR measure indirectly the grid stability, not much consensus is observed in the EC research community when it comes to find an appropriate metric to account for the grid stability. In terms of environmental analysis, the two main metrics used are CO2 emissions savings and GHG emissions savings. The social aspect remains rarely investigated regarding ECs.

4.5.1 Self-consumption and self-sufficiency

With no energy storage, the self-consumption (E_{SC}) and self-sufficiency (E_{SS}) energy values are the same and can be calculated using Equation 9. E_{SC} and E_{SS} are limited by whichever of the load and the self-generated energy is the smallest.

$$E_{SC}(t) = E_{SS}(t) = min\{E_{load}(t); E_{PV,gen}(t)\} \tag{9}$$

where E_{load} is the electricity demand and $E_{PV,gen}$ is the self-generated energy.

In the case of energy storage, Equation 9 splits into Equation 10 and Equation 11 since E_{SC} and E_{SS} are no longer the same. The battery charging is considered as self-consumption energy while the battery discharging is considered as self-sufficiency energy. These equations are taken from the modeling equations in the software Polysun [84].

$$E_{SC}(t) = min\{E_{load}(t) + E_{chg}(t); E_{PV,gen}(t)\} \tag{10}$$

$$E_{SS}(t) = min\{E_{load}(t); E_{PV,gen}(t) + E_{dchg}(t)\} \tag{11}$$

where $E_{chg}(t)$ is the self-generated energy charged in the battery storage and $E_{dchg}(t)$ is the energy discharged from the battery storage.

The SCR is defined as the share of self-generated energy that is self-consumed, either directly or by means of previous storage, following Equation 12. Therefore, the complementary of the SCR is the share of self-generated energy that is fed-back to the grid. The SSR is defined as the share of electricity demand that is actually covered by self-generated energy, following Equation 13. It gives an idea of the how relevant is the self-consumed energy in the electricity demand. Therefore, the complementary of the SSR is the share of electricity demand that is taken from the grid. Typically, for low installed capacities, the SCR is high because most of the self-generated energy is self-consumed, but the SSR is low since the self-consumed energy does not cover a significant share of the electricity demand. As the installed capacity increases, more electricity demand is covered with self-consumed energy, increasing the SSR, but because of the nature of solar energy (see Figure 15a), more excess

energy also takes place, decreasing the SCR. Therefore, SCR and SSR are typically opposing (see Figure 15b). The SCR gets lower and lower the more capacity installed, which typically entails more surplus energy. However, the SSR does not increase endlessly if the capacity increases. It reaches a maximum value when the maximum load-match has been achieved. Here, more capacity only leads to more surplus energy, not to demand coverage. This threshold value in SSR is not observed in the scheme of Figure 15b, but it is frequently observed in the publications that use SSR as a PV performance metric, such as the work made by Jiménez-Castillo et al. [85].

$$SCR(\%) = \frac{\sum E_{SC}(t)}{\sum E_{PV,gen}(t)} \times 100 \tag{12}$$

$$SSR(\%) = \frac{\sum E_{SS}(t)}{\sum E_{load}(t)} \times 100 \tag{13}$$

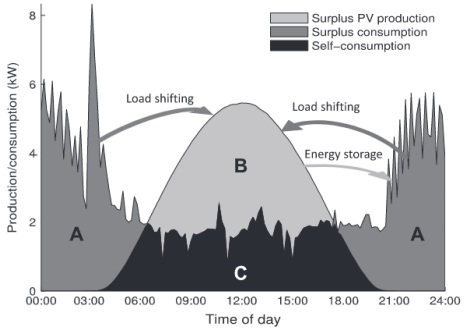

(a) Schematic outline of daily electricity demand (A+C) and self-generation (B+C) in a sunny day [17].

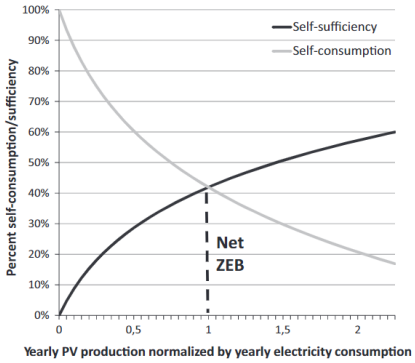

(b) Example of the relation between SCR and SSR [17].

Figure 15: None of the Y axis must be understood as fractions. On the left, SCR=C/(B+C) and SSR=C/(A+C). Two mechanisms to enhance self-consumption are shown: energy storage and load shifting. Other alternatives are implicit storage, energy sharing or having multiple tilts/orientations. On the right, the Net Zero Energy Building (Net ZEB) point is shown, for which SCR=SSR. This means that the self-generated energy equals the electricity demand, but over the course of a certain time (e.g. 1 year), allowing energy exchanges with the grid (imports or exports) when needed. This situation must not be confused with a perfect load-match for every time slot, an ideal situation for which SCR=SSR=100% and where no energy exchanges with the grid are needed, achieving a complete independence from the grid.

The electricity provided by the grid is usually linked to fossil fuels and GHG emissions, so a high SSR is convenient from an ecological perspective. On the other hand, large amounts of energy fed-back to the grid (at peak generation times) leads to voltage violations and line overload, so a high SCR is convenient for from a grid stability perspective. However, because SCR and SSR are typically opposing, a trade-off between a high SSR and high grid stability is therefore established [34]. From an economic perspective, a high SSR is convenient since the self-generated PV energy is usually cheaper than the provided by the grid, although this depends mainly on the amortization of the PV investment costs (pay-back time). Whether a high SCR is convenient or not from an economic perspective depends on the value given to the surplus energy, which is typically given by the FiTs [85]. The decreasing value given to the surplus energy, either by decreasing FiTs (mainly due to limited public budget) or by ongoing economic penalties for low SCRs (mainly targeted to avoid extra reinforcement costs in a high PV penetration context), suggests that a high SCR may

also lead to economic benefits.

A SCR and SSR of to 100% means that the self-generated energy is exactly the same as the self-consumed energy for each time slot, and this covers the whole electricity demand. In this ideal scenario, no energy is either taken or fed-back to the grid. However, keeping both rates at high values is challenging, especially in the high PV penetration scenario expected for the future. This can be achieved by the mechanisms introduced in Chapter 1.4, such as storage with a smart operating management, implicit storage (PV oversizing and curtailment of surplus energy), energy sharing (in ECs for instance), load-matching using different tilts and orientations, demand flexibility (load shifting) or blending optimally PV energy with other complementary renewable sources, such as wind energy. Another option would be to increase the grid network capacity and balancing mechanisms to handle the high PV penetration, but this is assumed to be excessively costly, in economic and planning terms.

In Equation 12 and 13, the typical summation period is 1 year, which is sufficiently long to take seasonal variations into account and to minimize the influence of short-term random fluctuations in generation and demand. By doing long-term simulations, every time of the year is simulated or measured. This is of high importance especially for countries at high latitudes with a considerable seasonal variation in solar irradiation, which strongly affects the PV production and thus the self-consumption. The present report uses hourly-based meteorological data and load consumption data for availability and computation reasons, but a larger time resolution (sub-hourly time-steps) is highly recommended when self-consumption targets are aimed [17]. Otherwise the instantaneous peak variability of the load consumption profiles and those of the PV generation profiles are smoothed and hence disregarded. The load consumption profile typically causes a larger error in this sense because it is more abrupt than the PV generation profile. The lower the time resolution, the more unrealistically smooth become both profiles, increasing the load match and finally leading to overrated values of SCR and SSR [85].

4.5.2 Grid stability

The energy exported to the grid (E_{exp}) and imported from the grid (E_{imp}) can be calculated as:

$$E_{exp}(t) = E_{PV,gen}(t) - E_{SC}(t) \tag{14}$$

$$E_{imp}(t) = E_{load}(t) - E_{SS}(t) \tag{15}$$

As explained above, the SCR and SSR give an idea of the grid stability, but a metric is needed that considers both the grid exports (like SCR) as well as the grid imports (like SSR). The Energy balance index (EBI), expressed in Equation 16, is used by Hutty et al. [19] to determine the grid stability. It is basically a measure of grid independence, penalising both grid imports and exports. Ideally, EBI is equal to 100%, which only occurs in the ideal scenario that SCR=SSR=100%. Similarly to SCR and SSR, a reasonable summation period in Equation 16 is 1 year and the higher the time resolution the better to account accurately for the peaks in energy imports and exports.

$$EBI(\%) = \left[1 - \frac{\sum E_{imp}(t) + \sum E_{exp}(t)}{\sum E_{load}(t) + \sum E_{PV,gen}(t)}\right] \times 100 \tag{16}$$

For clarification, linked to the idea explained in the caption of Figure 15, SCR, SSR and EBI are metrics calculated from time-step-dependent values. Therefore, for example, if

one calculates EBI for just a two time-step period, $t = 1$ and $t = 2$, if $E_{imp}(1) = 10kWh$ and $E_{exp}(2) = 10kWh$, EBI is not 100%. This same concept applies as well for SCR and SSR. Moreover, SCR, SSR and EBI take into consideration the 'relevance' of each time step. Therefore, for example, if $E_{PV,gen}(1) = 5kWh$ and $E_{SC}(1) = 5kWh$, and $E_{PV,gen}(2) = 10kWh$ and $E_{SC}(2) = 0kWh$, SCR is not 50%. This same concept applies as well for SSR and EBI. These are the two reasons why EBI can be considered somehow a grid stability metric: because it considers the grid balance for each time step independently and it considers how much the imbalance weighs.

4.6 Optimization problem

An optimization problem is a mathematical problem that aims to find the best solution among all feasible solutions, where "best" is determined by a specific criterion or objective function. The objective function represents the quantity to be optimized, and it depends on a set of decision variables, which are the variables that can be adjusted to improve the objective function. The constraints are the conditions that the problem must satisfy. All solutions, optimal or not, that satisfy the constraints are encompassed in the so-called feasible space.

The goal of an optimization problem is to find the values of the decision variables that minimize or maximize the objective function while satisfying the constraints. The solution to an optimization problem can be either a local optimal solution or a global optimal solution. A local optimal solution is a solution that is optimal in a certain region of the feasible space but may not be the best solution overall. In contrast, a global optimal solution is a solution that is optimal for the entire feasible space and provides the best possible value of the objective function.

Relatively complex problems, such as the one tackled in this report, contain nonlinear and sometimes non-smooth functions. A non-smooth function is not differentiable at one or more points in its domain, or has a derivative that is not continuous at one or more points in its domain. Non-smooth functions may exhibit abrupt changes or kinks, resulting in non-differentiable or discontinuous points. Examples of non-smooth built-in functions in Excel are ABS, MIN or MAX. The most common discontinuous built-in function in Excel is the IF function. Among the three available optimization solvers in Excel, all developed by Frontline Systems [86], two are capable of dealing with nonlinearities: "GRG Nonlinear", meant for smooth problems, and "Evolutionary", meant for non-smooth problems. The remaining solver, "Linear LP", is meant for linear optimization problems.

"GRG Nonlinear" looks at the gradient (slope) of the objective function as the decision variables change to guide it towards a feasible and optimal solution. The algorithm cannot determine in which direction the function is increasing (or decreasing) in discontinuous or non-differentiable points in non-smooth functions. This is why "GRG Nonlinear" is not meant for non-smooth problems. Additionally, the solution obtained with this algorithm is highly dependent on the initial values of the decision variables and hence just a local optimal solution may be found if the problem is smooth but non-convex, as shown in Figure 16a. "GRG Nonlinear" includes a "multistart" option that can improve the prospects of finding a globally optimal solution. The "multistart" option will automatically run the GRG method from a number of starting points and will display the best of several locally optimal solutions found as the probable globally optimal solution. Because the starting points are selected at random and then "clustered" together, they will provide a reasonable degree of "coverage" of the space enclosed by the bounds on the variables. A GRG algorithm in the EC field is used by Awad and Gül [64] for instance.

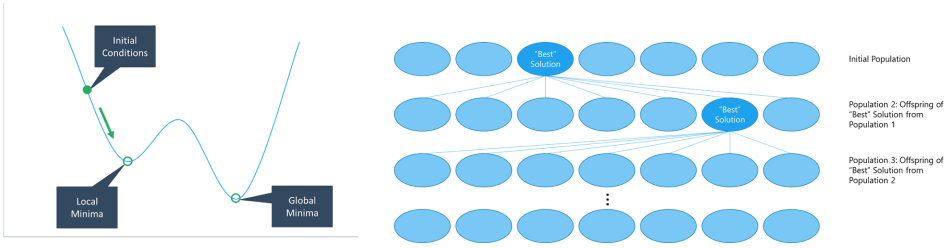

(a) GRG solver. (b) Evolutionary solver.

Figure 16: Scheme of the algorithms behind a Generalized Reduced Gradient (GRG) solver and an Evolutionary solver [87].

"Evolutionary" uses genetic and evolutionary algorithms. A genetic algorithm is a type of evolutionary algorithm. Both are inspired by natural selection and survival of the fittest in the biological world. Once the initial generation is randomly populated with members (sets of decision variables), the algorithm enters a loop that mimics the natural iterative process of new generations replacing old ones, as shown in Figure 16b. For each generation, based on natural selection, only the most "fit" member survives, but the other members of the population are sample points in other regions of the search space, where a better solution may later be found. Indeed, each generation is populated based on crossovers with previous existing solutions, (intentional changes based on survival), but also on mutations (random changes). This helps avoid becoming trapped at a local optimum, when an even better optimum may be found outside the vicinity of the current solution. "Evolutionary" is therefore more likely to find a globally optimum solution than "GRG Nonlinear" but is a much slower solving method. While "GRG Nonlinear" can be certain of the "optimality" of a certain solution by using gradient information, "Evolutionary" does not have any way to test whether a solution is optimal or not more than comparing it with others. A genetic algorithm in the EC field is used by Freitas et al. [34] for instance.

4.7 Roof pitch factor

The surface of a rectangular pitched roof, either single or doubled-pitched, can be determined using the so-called roof pitch factor, which is only dependent on the roof tilt (pitch) angle, following Equation 17.

$$\text{Roof pitch factor} = \frac{\text{Rafter}}{\text{Run}} = \frac{1}{cos\beta} \tag{17}$$

where β is the roof tilt angle. The lengths of the rafter and run of a roof are shown in Figure 17. Using this equation, the roof pitch factor values for some roof tilt (pitch) angles are shown in Table 1.

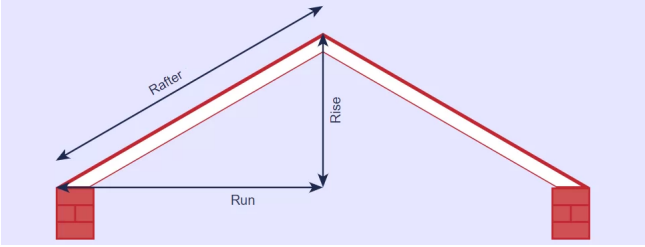

Figure 17: Overview of the roof lengths required to calculate the roof pitch factor. The roof tilt angle (β) is the angle between the rafter and the run [88].

Table 1: Roof pitch factor values for various roof tilt angles.

Tilt	Roof pitch factor
0°	1
20°	1.02
40°	1.15
60°	2

The roof surface can be then calculated using Equation 18. Hence, if the ground area of a certain building is known, the roof surface only depends on the roof pitch factor, which is given for a certain roof tilt angle.

$$\text{Roof surface} = \text{Roof pitch factor} \times \text{Ground area} \tag{18}$$

5 Methodology

The aim of this report is to provide technical advice to facilitate the decision-making regarding the PV installation in a residential EC. A model is developed in Excel and validated, and applied to a PV EC that will be built in Harstad, Norway [2]. More details about the objectives are explained in Chapter 3.2, as well as a brief and panoramic description of the methodology followed.

5.1 Weather data

The EC will be built in a specific address in Harstad, which is a municipality located in the Troms og Finnmark county in Norway. The location of Harstad within the Nordic region is shown in Figure 18.

Figure 18: The white area is the whole country of Norway. The arrow indicates the location of Harstad (68°N 16°E), which is above the Arctic Circle.

1-year hourly PV solar radiation data (GHI, DNI and DHI) is downloaded from the European tool Photovoltaic Geographical Information System ([89]: Typical Meterorological Year (TMY) from PVGIS-ERA5 2005-2020). The 'Calculated horizon' checkbox was kept selected in this tool to consider the orography of the specific location, which has an altitude of 20 m.a.s.l. This downloaded weather data also contains the hourly air temperature, relative humidity, infrared (thermal) radiation, wind speed and air pressure.

Since the weather data from [89] does not include any snow depth data, this is downloaded from [90] for a weather station located in Harstad Stadion. This weather station is very close to the specific location (less than 10km) and is located at an altitude of 45 m.a.s.l. Hourly snow depth data from the last 5 years (2019-2023, both included) is averaged and added to the weather file (see Figure 19).

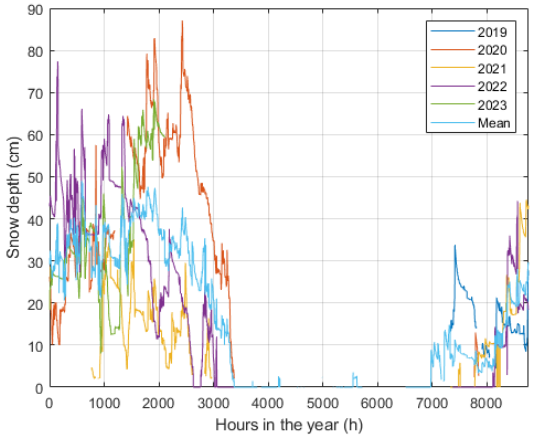

Figure 19: Hourly snow depth data in a weather station located in Harstad Stadion [90].

The albedo coefficient is not provided either in [89]. It is derived in an hourly basis by assuming its value to be 0.65 when there is any snow (snow depth not equal to 0) and 0.2 when there is no snow (snow depth equal to 0). The value of 0.65 is estimated based on the study made by Gardner and Sharp [78] while 0.2 is assumed for most of the PV system installed in urban environments [77]. The resulting albedo coefficients are added to the weather file.

5.2 Load consumption

Because the EC has not been built yet, no historic electricity consumptions of the households forming the EC exist. However, historic data of one household (the 'real' household) in the same neighborhood where the EC will be built is known. This household is 200m^2 and is inhabited by a family of 2 adults and 2 children. The hourly load profile for the last 3 years (2020, 2021 and 2022) is known. These three years are averaged and a 'real' consumption profile is obtained.

The other 99 electricity consumption profiles (the EC is formed by 100 households) are generated using the software Load Profile Generator [91]. This software allows to generate individual and realistic load profiles for households. The software's basic model is described in Figure 20. Based on their Desires, Persons will select what to do in the Household depending on the available Affordances (Activities). Desires have a certain weight and Persons decide on which Affordance to choose based on what would give them the maximum improvement in well-being at each time step. The Affordances available depend on the Devices available in the Household. Each Device use causes a certain energy use based on the Load Type and the Time Profile. All these elements can be created and customized by the user, but the software contains a large database for all elements. In the software 60 predefined Households for Germany are included. The author states that the predefined Households are based on a small survey, personal life experience, and statistical data in Germany and that they reflect slightly idealized versions of real behavior in northern Europe.

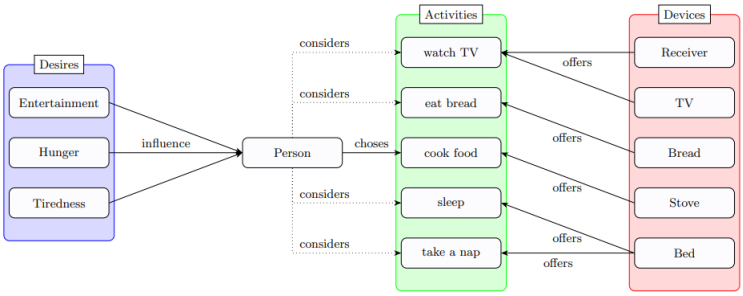

Figure 20: Interaction of key elements in Load Profile Generator. The Household is the central element in the model where all these key elements are put together. The manual can be found in Appendix B in [92].

The software allows to generate a large number of unique Households by creating Settlements. The Household templates and Settlement templates provide a way to automatically generate entire Settlements according to a number of rules to which the Households should conform. The program either finds predefined Households that conform to these rules or creates new ones. The program ensures that every Household is used only once in the created Settlement. A Settlement is used to generate the remaining 99 electricity consumption profiles (see Figures 21a and 21b). The decision-making internal time resolution in the software is set to 1min, but the resulting electricity consumption profiles are obtained in an hourly basis to match the weather data, which is also hourly.

The Settlement uses daily average air temperature and hourly solar radiation data (GHI) as input. These are available from the downloaded weather file mentioned in Chapter 5.1. The EC is expected to be occupied by Norwegian families (parents and children). A small study is carried out with data from [93] (more specifically, Table no 06242) to estimate how many children must live in each household. In Harstad's county, Troms until 2019 and Troms og Finnmark from 2020, in the last ten years (2012-2022), there were on average 21% of children with no siblings, 45% children with one sibling, 25% children with two siblings, 7% children with 3 siblings, 2% children with 4 siblings and 1% children with 5 siblings or more. The sum of these percentages values adds up 101% due to integer rounding. This statistic data was used in the created Settlement, although for simplicity in the software, the shares of children with 3, 4 and 5 or more siblings were added up (10%) and simulated as multi-generational families with two children and two seniors.

The generated hourly-based 99 load consumption profiles and the 'real' consumption profile are added up to create an EC aggregated electricity consumption of 100 households. However, although the 99 generated profiles (peaks) are fairly realistic, their total consumption values are not. This is why the previous aggregated EC consumption profile is scaled to the monthly total consumption values of the 'real' consumption times 100 (see Figures 21c and 21d). This is done using a scaling tool in SAM. The result is hence a final EC electricity consumption formed by 100 different hourly load profiles (different hourly peaks) with same total consumptions equal to the 'real' consumption.

(a) Day-averaged load profiles (before scaling). Blue lines: 99 generated load profiles. Dashed black line: averaged load profile. Dashed gray line: 'real' load profile.

(b) Month-averaged load profiles (before scaling). Blue lines: 99 generated load profiles. Dashed black line: averaged load profile. Dashed gray line: 'real' load profile.

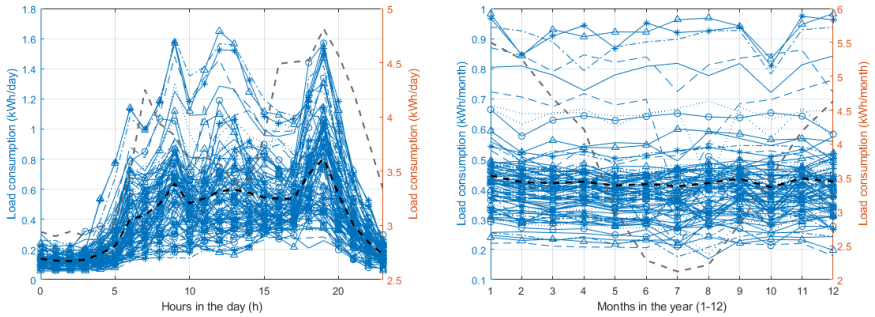

(c) Day-averaged aggregated EC load profile scaled to the 'real' load profile.

(d) Month-averaged aggregated EC load profile scaled to the 'real' load profile.

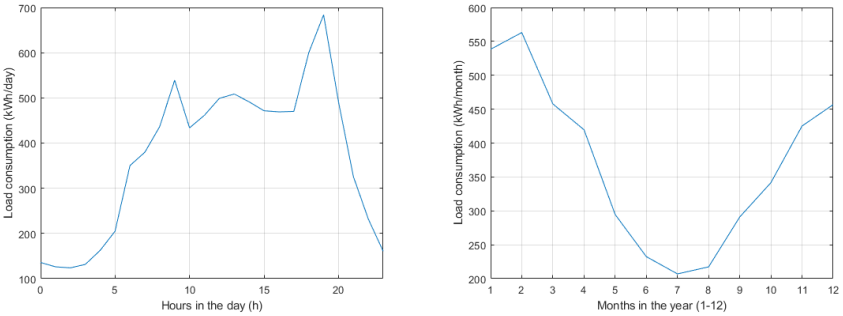

Figure 21: EC load consumption profiles.

5.3 PV generation

The models mentioned in this chapter have already been introduced in Chapter 4. The PV electricity generation is calculated in SAM in kWh/m^2 units for each hourly time step in the year and for each available orientation/tilt combination for potential PV installation in the EC. Since the EC is not built yet, the orientations and tilts considered are various: tilt angles of 0°, 20°, 40° and 60° and orientation angles corresponding to the four cardinal directions (north (N), south (S), east (E) and west (W)), leading to 13 possible combinations. It is reminded that if the tilt angle is 0°, no orientation can be considered.

To this end, the Perez model is selected in SAM to transpose the solar data from the weather file into the plane-of-array diffuse radiation. The direct-beam and ground-reflected radiation are calculated in SAM as described in Equation 3. The "CEC Performance Model with User Entered Specifications" is selected in SAM as the module's performance model [69]. This six-parameter model allows the user to enter the module's STC specifications and uses the Dobos calculator to calculate the STC model parameters. This model takes into consideration the reflection losses. The module STC specifications provided in the manufacturer's data sheet as well as the resulting module's performance model parameters are shown in Table 2.

Table 2: Left: Module STC specifications from manufacturer's data sheet [94]. Right: Derived CEC model parameters at STC using Dobos calculator in SAM.

V_{mp}	34.17V
I_{mp}	9.95A
P_{mp}	340W
V_{oc}	42.41V
I_{sc}	10.52A
η	20.22%
α	0.046%/°C
β	-0.276%/°C
γ	-0.381%/°C
A	1.68m^2

a	1.64V
I_L	10.88A
I_0	5.74E-11A
R_s	0.33 Ohm
R_{sh}	89.20 Ohm
$adjust$	12.65%

The parameter *adjust* is not part of the five-parameter Single-diode model and is therefore specific to the CEC model. α and β are adjusted by this parameter until γ in the data sheet matches the γ predicted by the six-parameter CEC model [75].

The "CEC Performance Model with User Entered Specifications" uses the NOCT temperature model to estimate the temperature of the module. To this end, it is required by SAM to enter the "Array height", which is selected as "two stories or higher", and the Mounting standoff, which is assumed to be "1.5 to 2.5 inches".

Snow coverage losses are included in the model using SAM's snow model, which is based on the Marion model (see Figure 22). It uses snow depth data from the input weather file, and for time-steps with snow, estimates the percentage of the photovoltaic array that is covered with snow based on the array's tilt angle, plane-of-array irradiance, and ambient temperature [69].

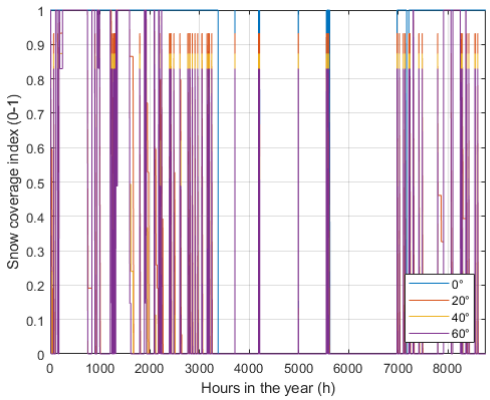

Figure 22: Snow coverage index for the 4 tilts considered. An index of 1 means that the PV module is fully covered with snow. The snow coverage index mean values are 0.59, 0.24, 0.19 and 0.18 for a tilt of 0°, 20°, 40° and 60°, respectively.

The soiling losses are assumed to be constant and equal to 1.5% based on the study made by Pedersen et al. [83]. The values given by SAM for DC power loss (4.4%) and AC power loss (1%) are maintained. A constant inverter efficiency of 96% is considered, based on the work by Cillari et al. [95]. No further inverter modeling is considered for simplicity and because the optimization solver used (explained later in Chapter 5.5) will iterate among multiple PV capacities installed, and hence specifying inverter nominal or extreme voltage/current values would lead to unrealistic clipping losses.

Figure 23 shows the PV generation over a 1-year period for the 13 different orientation/tilt combinations considered in the optimization problem. It is observed that steep tilts and south and east orientations lead to a larger PV generation.

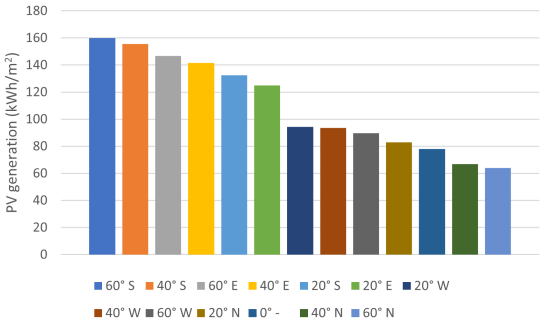

Figure 23: 1-year total PV generation. Nomenclature: for instance, "60° S" means a tilt of 60° and a south orientation.

5.4 Battery energy storage

The battery modeling equations shown in this chapter, together with the equations described in Chapters 4.5.1 and 4.5.2, define the energy inflows and outflows for each time-step (to/from battery, to/from load, to/from grid) and the key performance metrics (SCR, SSR and EBI). The battery capacity is inputted in the Excel optimization problem in kWh/kWp units where kWp is the optimal PV capacity found by the Excel solver. Five different battery sizes are considered, leading to five different scenarios: 0, 0.25, 0.5, 0.75 and 1 kWh/kWp.

The equations shown below describe the battery functioning and are inspired from the modeling equations used in the softwares Polysun [84] and SAM [69]. It is assumed that the battery is AC coupled, as shown in Figure 24. It is also assumed that it operates at a constant (nominal) voltage with a non-smart management strategy. No thermal or degradation losses are considered. It is reminded that the PV simulation period is 1 year and the time resolution is hourly-based (8760 time-steps in the year).

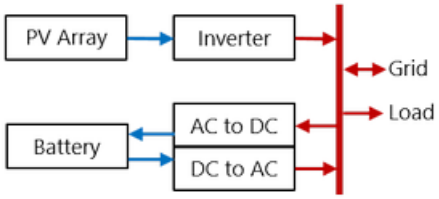

Figure 24: Scheme of an AC coupled battery in a PV system. Blue: DC side. Red: AC side. [69]. See also Figure 10.

A non-smart management strategy means that the battery is charged whenever there is surplus PV generation in a given time step and is discharged whenever the PV generation is not enough to cover the electricity demand, as described by Equations 19 and 20. If the battery is fully charged and there is still surplus energy, this energy is fed-back to the grid. If the battery is fully discharged and the electricity demand is not met, this energy is taken from the grid. The battery cannot charge and discharge in the same time step.

$$\text{DC side: } E_{chg,DC}(t) = min\{E_{net}(t)\eta_{chg}; E_{chg,max}(t)\} \text{ if } E_{net}(t) > 0 \tag{19}$$

$$\text{DC side: } E_{dchg,DC}(t) = min\{-E_{net}(t)/\eta_{dchg}; E_{dchg,max}(t)\} \text{ if } E_{net}(t) < 0 \tag{20}$$

where $E_{net}(t) = E_{PV,gen}(t) - E_{load}(t)$, η_{chg} and η_{dchg} are the charging/discharging efficiencies, and $E_{chg,max}(t)$ and $E_{dchg,max}(t)$ are the maximum possible charge/discharge values, described by Equations 21 and 22 (see Figure 25). The maximum charge/discharge occurs for a certain time step when either (i) the maximum/minimum state of charge (SOC_{max} and SOC_{min}) has been achieved, or (ii) the maximum charging/discharging rate (C_{chg} and C_{dchg}) has been achieved:

$$E_{chg,max}(t) = min\{SOC_{max}Cap_{batt} - E_{SOC}(t-1); Cap_{batt}C_{chg}\} \tag{21}$$

$$E_{dchg,max}(t) = min\{E_{SOC}(t-1) - SOC_{min}Cap_{batt}; Cap_{batt}C_{dchg}\} \tag{22}$$

where Cap_{batt} is the battery capacity (in kWh), and $E_{SOC}(t)$ is the energy available in the battery (in kWh), given by Equation 23. The $SOC(t)$ itself, meaning the energy available in the battery normalized to the battery capacity (in %), can be calculated by Equation 24.

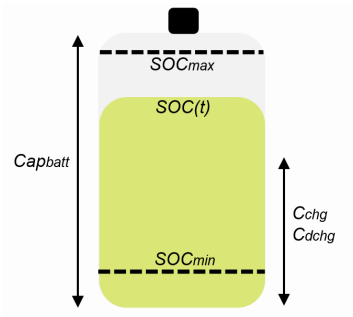

Figure 25: Scheme of some key parameters in the battery.

$$E_{SOC}(t) = E_{SOC}(t-1) + E_{chg,DC}(t) - E_{dchg,DC}(t) \tag{23}$$

$$SOC(t) = \frac{E_{SOC}(t)}{Cap_{batt}} \times 100 \tag{24}$$

The first time step ($t = 1$) is slightly different from all the rest since the term $E_{SOC}(t-1)$ in the previous equations is replaced by SOC_{ini}*Cap_{batt}, where SOC_{ini} is the initial state of charge (in %).

Equations 19 and 20 account for the DC side. The charging and discharging values for the AC side are given by the charging/discharging efficiencies:

$$\text{AC side: } E_{chg,AC}(t) = E_{chg,DC}(t)/\eta_{chg} \tag{25}$$

$$\text{AC side: } E_{dchg,AC}(t) = E_{dchg,DC}(t)\eta_{dchg} \tag{26}$$

The specific parameter values in the battery are given in Table 3.

Table 3: Battery parameters, based on the work by Freitas et al. [34]. Five scenarios are considered with different battery capacities, Cap_{batt}: 0, 0.25, 0.5, 0.75 and 1 kWh/kWp, where kWp is the optimal PV capacity found by the Excel solver (see next chapter).

SOC_{ini}	50%
SOC_{min}	10%
SOC_{max}	95%
C_{chg} and C_{dchg}	0.5
η_{chg} (AC to DC) and η_{dchg} (DC to AC)	95%

5.5 Optimization problem

The developed Excel optimization model uses as input: (i) the 1-year hourly PV generation data extracted from SAM in kWh/m^2 units for each available orientation/tilt combination for potential PV installation in the EC (see Chapter 5.3), and (ii) the 1-year hourly EC demand profile in kWh units generated with Load Profile Generator and scaled with SAM (see Chapter 5.2). The hourly overall PV generation, i.e. considering all orientation/tilt combinations, is obtained simply by adding up the contribution of each orientation/tilt combination.

The battery model equations are included in the Excel model (see Chapter 5.4), as well as the equations described in Chapters 4.5.1 and 4.5.2. These equations define the energy inflows and outflows for each time-step (to/from battery, to/from load, to/from grid) and the key performance metrics (SCR, SSR and EBI). The Excel solver is then run to find the optimal roof surface area in m^2 that may be equipped with PV for each orientation/tilt combination in order to maximize the objective functions, which are defined later in this chapter. The resulting optimal PV area can be easily translated into PV capacity (in kWp units) for the given 20.22% module efficiency (see Table 2) using Equation 4, or even into equivalent number of houses (roofs) fully covered with PV, given the roof surface of 1 house, which only depends on the tilt angle using Equation 18.

Two objective functions are considered: one that focuses on SCR and SSR (Equation 27), and one that focuses on EBI (Equation 28). The latter simply maximizes EBI. In the former, instead of using SCR and SSR as individual objective functions, the multi-objective function shown in Equation 27 is chosen because SCR and SSR are by definition opposing (see Figure 15b). The use of the weights a and b give a panoramic picture of the system performance, considering multiple self-consumption possibilities. This facilitates the PV sizing decision-making depending on the EC energy goals and requirements, which are unknown.

$$f_1 = a \cdot SCR + b \cdot SSR \tag{27}$$

$$f_2 = EBI \tag{28}$$

where a and b are the weights given to each metric in the optimization. These weights are both between 0 and 1 and must add up 1, i.e. $0 \leq a, b \leq 1$ and $a + b = 1$. The a values selected are 0, 0.25, 0.5, 0.75 and 1.

Table 4 shows an overview of all the different scenarios considered. For each of this scenarios there are 13 decision variables, which are the PV installed capacity for the 13 orientation/tilt combinations considered: tilt angles of 0°, 20°, 40° and 60° and orientation angles corresponding to the four cardinal directions (north, south, east and west). The output results

of each scenario is the optimal PV installed capacity and the performance metrics SCR, SSR and EBI.

Table 4: All scenarios considered in the optimization problem.

Scenarios		Battery capacity (kWh/kWp)				
		0	0.25	0.5	0.75	1
Objective function	f_1	a = 0	a = 0	a = 0	a = 0	a = 0
		a = 0.25	a = 0.25	a = 0.25	a = 0.25	a = 0.25
		a = 0.5	a = 0.5	a = 0.5	a = 0.5	a = 0.5
		a = 0.75	a = 0.75	a = 0.75	a = 0.75	a = 0.75
		a = 1	a = 1	a = 1	a = 1	a = 1
	f_2	-	-	-	-	-

The only constraint of the problem is the roof surface available in m^2 units for each orientation/tilt combination. It is assumed that all households cover a rectangular ground area of 200m^2, like the 'real' household. The roof pitch factor for each tilt angle (see Chapter 4.7) and the fact that the EC is formed by 100 households allows to define the roof availability constraint.

It is clear the non-linearity and non-convexity of the objective functions, given the definitions of SCR, SSR and EBI (see Chapters 4.5.1 and 4.5.2), and the battery modeling equations (see Chapter 5.4). The formulation of the problem includes Excel built-in functions typical of non-smooth problems as well, such as MIN or IF, but the objective functions themselves seems to be smooth with respect to the decision variables. The problem is solved using the solver "GRG Nonlinear with multistart". However, the solver "Evolutionary" is run for different scenarios to confirm that the solutions given by "GRG Nonlinear with multistart" are reliable and not local optimal solutions. This analysis is done in Chapter 6.4, where a validation of the model developed and the optimization results is carried out. The specific solver parameters selected in Excel are shown in Table 5. These parameters are based on multiple trial and error attempts to determine which parameters lead to reliable and accurate PV optimal capacities. The population size is based on the number of decision variables (13) multiplied by 10, as suggested by the developers of the Excel optimization solvers, Frontline Systems, in [96] ("GRG" parameters) and [97] ("Evolutionary" parameters).

Table 5: Excel solver parameters.

	GRG	**Evolutionary**
Constraint precision	0.001	0.001
Convergence	0.01	0.00001
Solving time	0.5h	1.5h
Population size	130	130
Mutation rate	-	0.075 (default)

6 Results discussion and validation

6.1 Results description

Before presenting and discussing the results, it must be highlighted that the installed PV capacity is not shown in any figure in kWp or m^2 units, but in number of houses fully covered with PV. This is intended to help interpreting the results. It is reminded that it is assumed that all households cover a rectangular ground area of 200m^2, like the 'real' household. The roof pitch factor for each tilt angle (see Chapter 4.7) allows to calculate the roof surface available for each house depending on the tilt angle of the roof. The area of one PV module (see Table 2) allows to calculate the roof surface (in number of houses) that is covered with PV. The goal of the Excel solver is to find the optimal PV capacity for each orientation/tilt combination, for certain given energy goals (defined by f_1 and f_2) and certain battery capacity values.

Figures 26 and 27 are result of solving the optimization problem with f_1 as objective function, whereas Figure 28 is result of solving the optimization problem with f_2 as objective function. Figures 29 and 30 are not result of solving the optimization problem, but figures to have a better understanding of the other figures.

Since in f_1 the a values that are considered are 0, 0.25, 0.5, 0.75 and 1, the corresponding b values are 1, 0.75, 0.5, 0.25 and 0, respectively. The graphs in Figure 26 are shown with respect to these a values. Since $f_1 = a \cdot SCR + b \cdot SSR$ where $0 \leq a, b \leq 1$ and $a + b = 1$, $a = 0$ ($b = 1$) means that the problem maximizes only SSR whereas $a = 1$ ($b = 0$) means that the problem maximizes only SCR. The a values between 0 and 1 (the b values between 1 and 0) give different weights to SCR and SSR. For instance, $a = 0.5$ ($b = 0.5$) give the same weight to SCR than to SSR. Two graphs (left and right) are shown for each battery capacity value in Figure 26. One graph (left) showing the the total installed PV capacity, the SCR, the SSR and the EBI, and the other graph (right) showing the distribution of orientation/tilts normalized to the total installed PV capacity. Since 5 different battery capacity values are considered (0, 0.25, 0.5, 0.75 and 1 kWh/kWp), there are five couple of graphs, a couple for each battery capacity. Note that the legend and caption of Figure 26 are one page below the graphs. The meaning of Figure 27 is to compare the outputs of each scenario when changing the battery capacity. This comparison is not well observed in Figure 26 because it shows separated graphs for different battery capacity values.

The way of showing the results when maximizing f_2 is different, as observed in Figure 28. Since there are no weights considered in this objective function, the results are directly shown with respect to the battery capacity values (whereas in Figures 26 and 27 the results were shown with respect to the a values). It is kept in Figure 28 the fact of showing a couple of graphs, one (left) with the total installed PV capacity, the SCR, the SSR and the EBI, and the other graph (right) with the distribution of orientation/tilts normalized to the total installed PV capacity.

Since the output results of each scenario (see Table 4) are the optimal PV installed capacities for each orientation/tilt combination (decision variables) and the performance metrics SCR, SSR and EBI (objective functions), the discussion of the results is divided in two parts: one focused on the latter (Chapter 6.2) and one focused on the former (Chapter 6.3).

(a) No storage

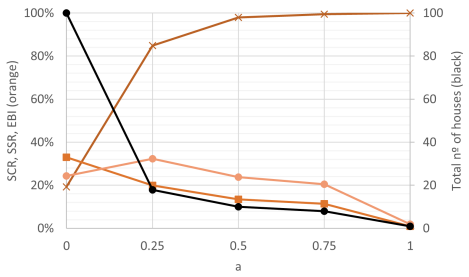

(b) No storage

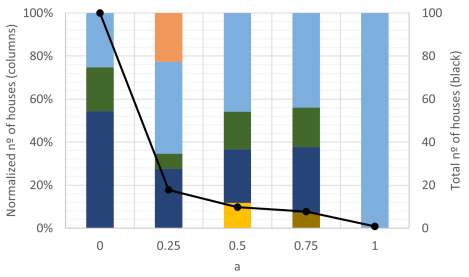

(c) 0.25 kWh/kWp

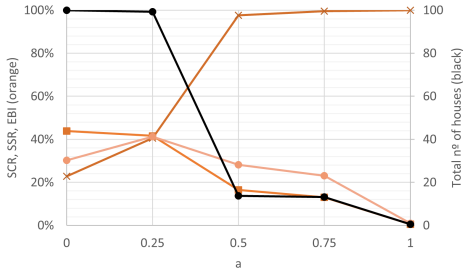

(d) 0.25 kWh/kWp

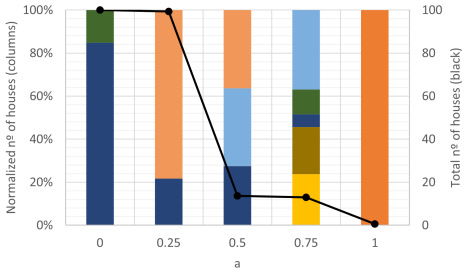

(e) 0.5 kWh/kWp

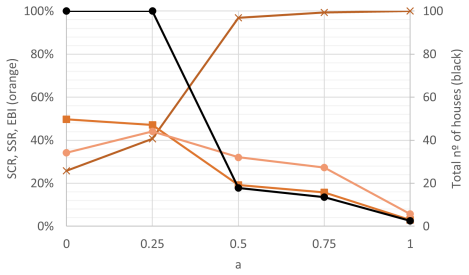

(f) 0.5 kWh/kWp

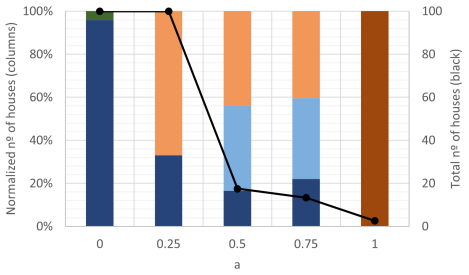

(g) 0.75 kWh/kWp

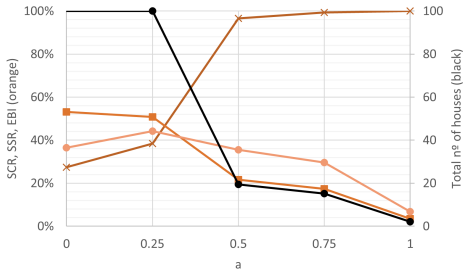

(h) 0.75 kWh/kWp

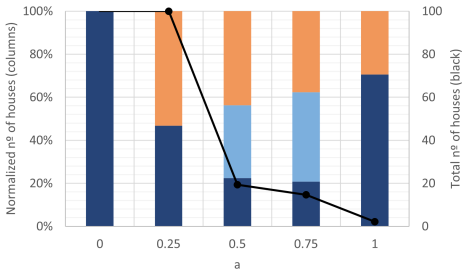

(i) 1 kWh/kWp

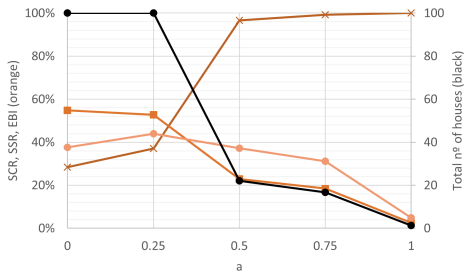

(j) 1 kWh/kWp

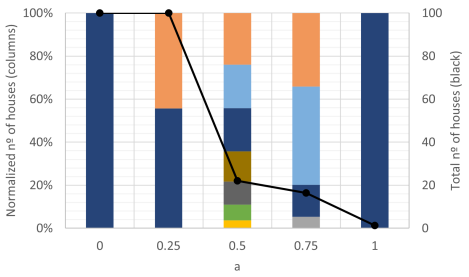

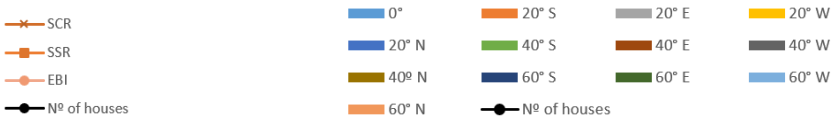

Figure 26: The graphs in this figure are result of maximizing $f_1 = a \cdot SCR + b \cdot SSR$ where $0 \leq a, b \leq 1$ and $a + b = 1$. Left column graphs: Total optimal installed PV capacity (black curve, right axis), SCR, SSR and EBI (orange curves, left axis) with respect to the a weight parameter for different storage capacities. Right column graphs: Total optimal installed PV capacity (black curve, right axis) and distribution of the orientation/tilt combinations covered with PV normalized to the total installed PV capacity (colored stacked chart, left axis) with respect to the a weight parameter for different storage capacities. The PV installed capacity, instead of being shown in kWp, is shown in number of houses fully covered with PV. Nomenclature: for instance, "60° S" means a tilt of 60° and a south orientation.

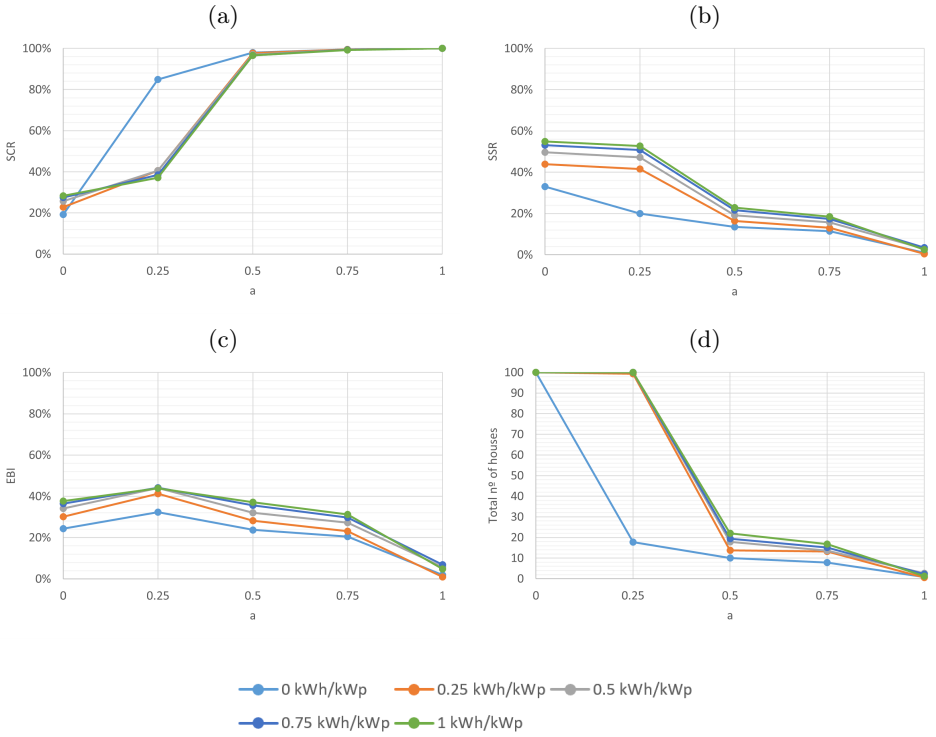

Figure 27: The graphs in this figure are result of maximizing $f_1 = a \cdot SCR + b \cdot SSR$ where $0 \leq a, b \leq 1$ and $a + b = 1$. SCR, SSR, EBI and total optimal installed PV capacity with respect to the a weight parameter for different storage capacities. The PV installed capacity, instead of being shown in kWp, is shown in number of houses fully covered with PV.

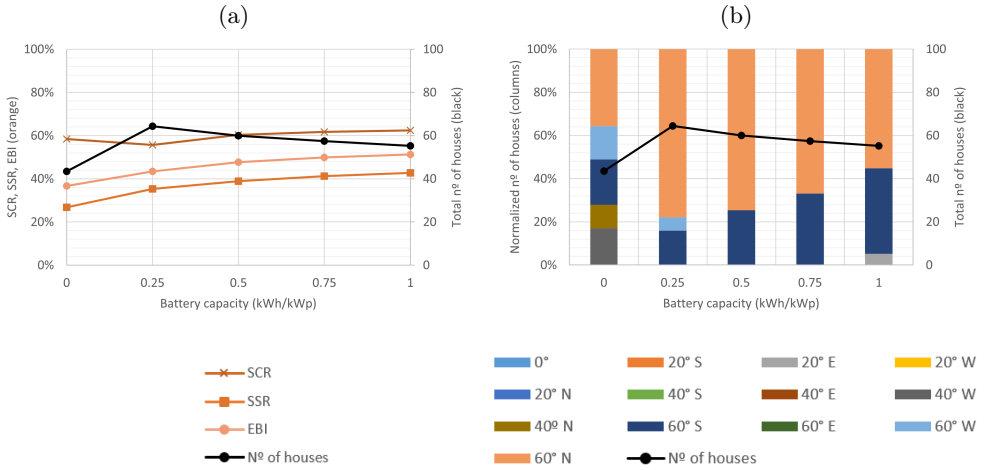

Figure 28: The graphs in this figure are result of maximizing $f_2 = EBI$. Left graph: Total optimal installed PV capacity (black curve, right axis), SCR, SSR and EBI (orange curves, left axis) with respect to the battery capacity. Right graph: Total optimal PV installed capacity (black curve, right axis) and distribution of the orientation/tilt combinations covered with PV normalized to the total installed PV capacity (colored stacked chart, left axis) with respect to the battery capacity. The PV installed capacity, instead of being shown in kWp, is shown in number of houses fully covered with PV. Nomenclature: for instance, "60° S" means a tilt of 60° and a south orientation.

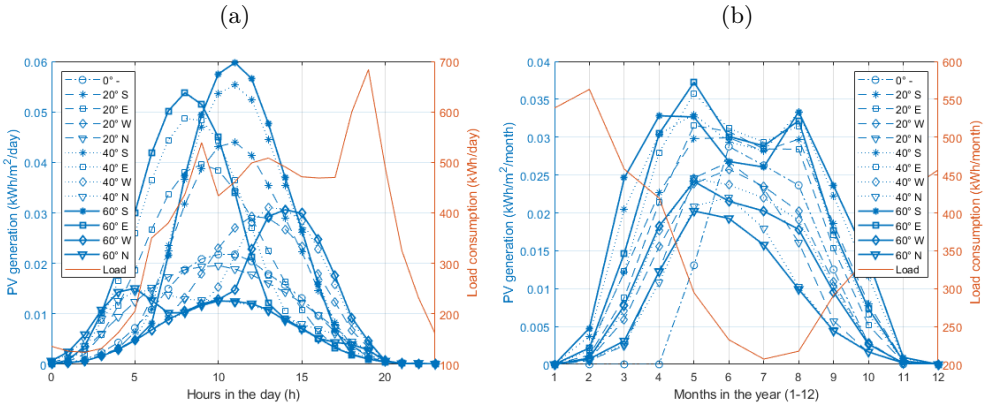

Figure 29: Daily (left graph) and monthly (right graph) averaged PV generation profiles (blue curves) and EC aggregated load consumption profile (red curve) for all tilts considered (0°, 20°, 40° and 60°) and the four different orientations considered (S,E,W and N). The most preferred tilt angle by the solver, 60°, is shown in bold and in separate graphs in Figure 34 in Appendix. Nomenclature: for instance, "60° S" means a tilt of 60° and a south orientation.

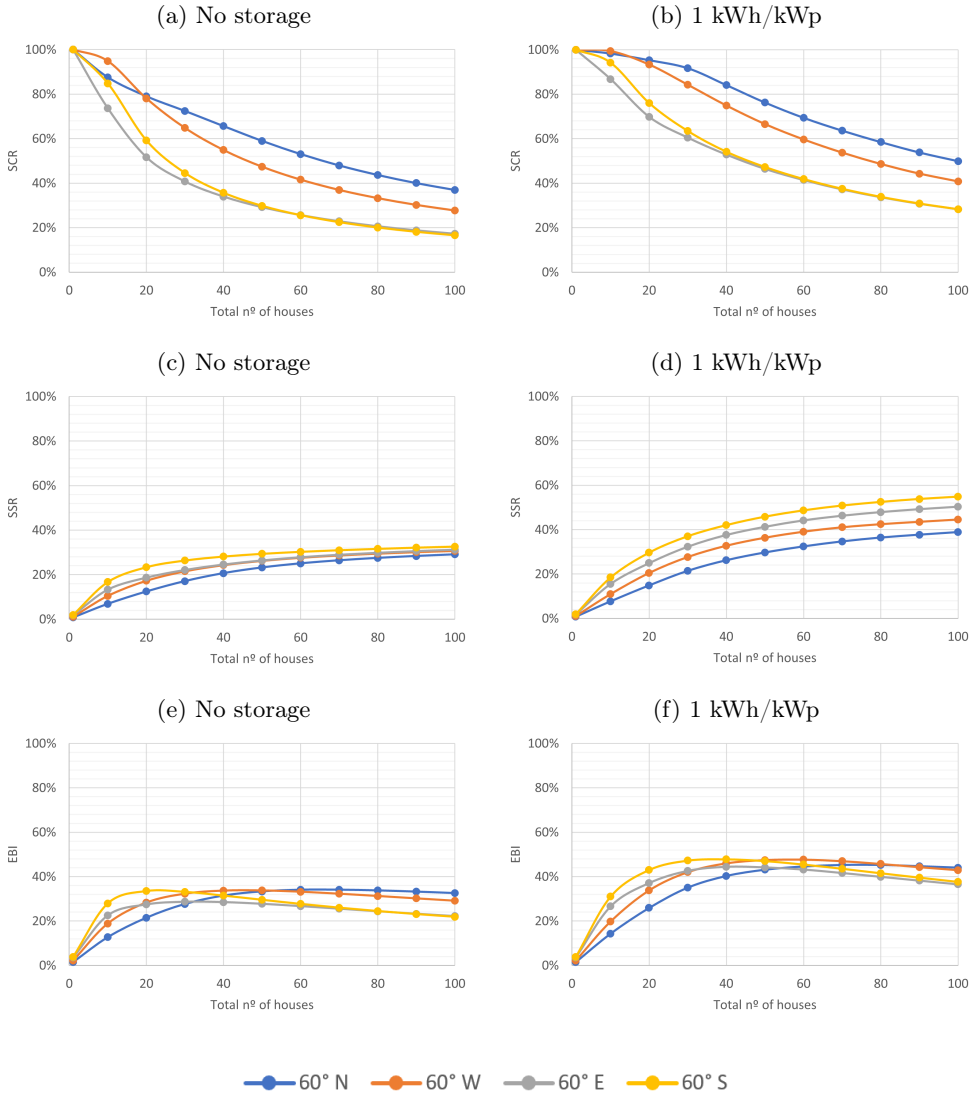

Figure 30: Evolution of SCR, SSR and EBI with total installed PV capacity for different orientations (color code) and a tilt of 60°, which is the main tilt angle chosen by the solver. Left graphs: No storage. Right graphs: Battery capacity of 1kWh/kWp. In these figures, for each orientation, PV is installed in just that orientation. The PV installed capacity, instead of being shown in kWp, is shown in number of houses fully covered with PV. Nomenclature: for instance, "60° S" means a tilt of 60° and a south orientation.

6.2 Discussion of SCR, SSR and EBI curves

The discussion starts with interpreting the curves from Figure 26a, which is the case of maximizing f_1 with no battery storage. The total installed capacity decreases when a increases. Increasing a means giving more weight to SCR in the optimization and less to SSR. In other words, increasing a helps having less amount of surplus energy with respect to the PV generated energy, increasing SCR, but also less amount of demand covered by PV energy (since b decreases), decreasing SSR. This is why the SCR curve increases with a and the SSR curve decreases with a. They way of increasing SSR is by increasing the total installed PV capacity, whereas the way of increasing SCR is by decreasing the total installed PV capacity, always considering optimal orientation/tilt combinations. Less PV capacity

covers less demand, decreasing SSR, but ensures less amounts of surplus energy, increasing SCR. If all the optimization weight is given to avoid surplus energy regardless of how much demand is covered by PV energy, which is represented by $a = 1$, the solver chooses to install almost no PV, to ensure that SCR is 100%. However, this means that SSR$\sim$0 since very little demand is covered with PV energy, and EBI$\sim$0 since almost all demand is covered with energy taken from the grid. However, SCR is 100% (or close) already for a values of 0.5. An $a = 0.5$ means that $b = 0.5$ as well (since $a + b = 1$), meaning that both SCR and SSR are evenly maximized by the optimization algorithm. If all weight is given to cover demand with PV energy regardless of how much energy is fed-back to the grid, which is represented by $a = 0$, the solver chooses to cover all houses with PV. Nevertheless, this just covers a $\sim$33% of electricity demand with PV energy. Although different orientations and tilts are considered, which enhances the load match, a higher SSR than $\sim$33% is impossible (with no storage), since the maximum load-match has been achieved. This threshold value has been introduced in Chapter 4.5.1.

The SCR when $a = 0$ is very low, slightly above 20%. Moreover, it is rather unreal to consider the possibility of covering all 100 houses with PV. A SCR of 20% means that 80% of the PV energy is fed-back to the grid. As soon as the a value increases to 0.25, giving some weight to self-consume the PV energy and not feeding so much energy back to the grid, the solver chooses to install much less PV capacity, around 20 houses fully covered with PV. At this point the SSR decreases from $\sim$33% to 20%, but the SCR already rises drastically above 80%. Moreover, it is observed that for $a = 0.25$ the EBI finds its maximum value, representing the point of maximum independence from the grid and potentially the best scenario in terms of grid stability. If the a value is further increased, to 0.5, the SCR rises to almost 100%, but the SSR drops to around 15% and hence the EBI drops to a similar value than if $a = 0$ because of the large amounts of energy taken from the grid (low SSR).

The two previous paragraphs were referring to Figure 26a. To discuss how having a battery storage affects the results, it is maybe easier to look at Figure 27 than comparing Figures 26a, 26c, 26e, 26g and 26i, since these show the change in battery capacity in different graphs, while Figure 27 shows the battery capacity increase in same graphs. In Figure 27, it stands out the no storage scenario for $a = 0.25$. The drastic decrease in total installed PV capacity (see Figure 27d) occurs from $a = 0.25$ to $a = 0.5$ if storage is considered whereas in the case of no storage this drastic decrease occurs before, from $a = 0$ to $a = 0.25$. This much lower installed capacity in the no storage case for $a = 0.25$ leads to a much higher SCR (Figure 27a), but a much lower SSR (Figure 27b) and EBI (Figure 27c) than in the case with storage. Storage allows for a larger installed PV capacity (indeed, all 100 houses fully covered with PV) to increase SSR while maintaining acceptable levels of SCR, whereas no storage requires to install small PV capacities (around 20 houses fully covered with PV) to achieve acceptable levels of SCR, detrimental to SSR. This is simply because the battery allows to store energy and hence to handle amounts of excess energy to meet the demand that are directly fed-back to the grid in the no storage case. As mentioned before, covering all 100 houses fully with PV may not be too realistic. An $a = 0.5$ allows for a reasonable PV installed capacity in the storage case, around 20 houses fully covered with PV, which increases to almost 100% the SCR, detrimental to SSR, that drops drastically to around 20%.

In general, Figure 27 shows that the system performance is better the larger the battery capacity. It is observed how, for any a value, with increased battery capacity, the total installed PV capacity increases in Figure 27d, as well the SSR and the EBI in Figures 27b and 27c, respectively. It is interesting to see in Figure 27a how the SCR barely changes with an increase in the battery capacity while the SSR does change in Figure 27b. This is because the larger installed PV capacity with a larger battery capacity causes a larger coverage of the electricity demand with PV energy (higher SSR) but also leads to more

surplus energy, not so much as to decrease SCR, but enough to prevent it from increasing. It is reminded that SCR represents the share of PV energy that is self-consumed. Despite SCR remains constant with an increase in battery capacity, SSR increases with an increase in battery capacity, reason for which EBI also increases with a battery capacity increase. It can be observed as well that the increases in installed PV capacity, SSR and EBI are not linear with the increase in battery capacity. The more battery capacity the less the increase in system performance, as if there was a battery capacity threshold value from which the system performance was not enhanced anymore. This battery capacity value seems to be 0.75 kWh/kWp. This can be attributed to a similar reason as the SSR threshold observed in Figure 26: the battery helps for a better load-match, but there is always some electricity demand that cannot be met by using reasonable amounts of battery capacities.

So far, the figures discussed (Figures 26 and 27) correspond to an optimization using $f_1 = a \cdot SCR + b \cdot SSR$ (with different weights) as the objective function . Figure 28 shows the results when the objective function to be optimized is $f_2 = EBI$. It must be highlighted that the X axis in this figure is no longer the a value, which is nonexistent in f_2, but the battery capacity values. If there is no storage, the combination of SCR and SSR that lead to the highest EBI are ∼60% and ∼25%, respectively, leading to an EBI of almost 40%. When the battery capacity is 0.25 kWh/kWp, which is the smallest battery capacity value considered, the solver decides to install more PV capacity, more than for any other battery capacity value. Because of this, the lowest SCR is obtained for this battery capacity value. This seems weird, but for this battery capacity value, the EBI value, which is the objective function and the only metric that the solver cares about when maximizing f_2, behaves coherently with the rest of EBI values when the battery capacity is changed, which adds coherence to the solution suggested by the solver. In general, the larger the battery capacity, the larger EBI, but this increase is not significant: EBI is slightly below 40% for no storage and only rises to 50% if the battery capacity is 1 kWh/kWp. This increase observed in EBI is more due to an increase in SSR than in SCR, since SCR remains rather constant (∼60%) with a battery capacity increase. This was also observed in Figure 27, when maximizing f_1, and discussed in the previous paragraph.

6.3 Discussion of the distribution of orientations and tilts

The right column graphs of Figure 26 and Figure 28 show the distribution of orientation/tilts suggested by the solver for the maximization of $f_1 = a \cdot SCR + b \cdot SSR$ and $f_2 = EBI$, respectively. Before any further discussion about these graphs is done, it must be observed that the solutions for $a = 1$ in Figure 26 (right column graphs) are negligible. For $a = 1$, the solver decides to install a very small PV capacity, close to 0, to ensure a SCR of 100%. Since $a = 1$, $b = 0$, meaning that the solver just cares about maximizing SCR regardless of how much electricity demand is covered by PV energy (SSR). In this scenario, the solver finds difficulties to choose among the different orientations and tilts available for PV installation, since any combination easily leads to a SCR of 100% (all PV energy is self-consumed) if a very small PV capacity is installed. This does not occur for any other a value since if $a \neq 1$ ($b \neq 0$), some weight is given to SSR and hence an optimal solution (combination of orientations and tilts) exists. Therefore, the solutions for $a = 1$ ($b = 0$) in Figures 26b, 26d, 26f, 26h and 26j can be ignored. It is still valuable to observe that the solver decides to install very small PV capacities if $a = 1$, which was already mentioned in Chapter 6.2 and adds reliability to the optimization algorithm.

In Figure 26 and Figure 28 (right column graphs) it can be observed that the solver generally suggests the steepest tilt angle considered, 60°, and many different orientation combinations. Because of the northern latitude, a steep tilt angle, such as 60°, leads to a larger yearly PV generation and produces a more uniform PV profile throughout the year than

lower tilt angles. The former can be observed in Figure 23 whereas the latter can be observed in Figure 29b and more clearly in the work made by Awad et al. [98]. The low solar altitudes observed in northern latitudes in Winter months are leveraged for PV generation if a steep tilt is considered, enabling the low altitude sun rays hit the module's surface. The ground-reflected solar radiation, which is significant in northern latitudes during winter months due to the continuous presence of snow on the ground, is larger for steeper tilts as well (see Chapter 4.2). Snow coverage losses are also reduced the steeper the tilt angle, as observed in Figure 22, which also helps increasing the PV generation.

Moreover, the more uniform PV generation throughout the year for steeper tilts is enhanced because lower tilt angles produce more PV generation than steep tilts during Summer months, due to the high solar altitudes and enlarged solar azimuth during these months in northern latitudes. For steeper tilt angles and during summer months, the Sun is more time 'behind' the module's surface than for lower tilt angles, reducing the PV generation. This is observed in Figure 29b. All in all, the larger yearly PV generation due to a larger PV production in Winter months and the more uniform PV profile throughout the year make steep tilt angles to be preferred by the solver since the consumption load is clearly much larger for Winter months than for Summer months, as observed in Figure 29b as well, enhancing the load-match. All these reasons for which steep tilts are more convenient in northern latitudes are observed and also described by Awad et al. [98].

Regarding the orientations chosen by the solver it is observed in Figure 26 (right column graphs) that south orientation is the most prominent if $a = 0$. An $a = 0$ means that the solver tries to cover as much demand as possible with PV energy (maximizing SSR) regardless of the amount of surplus energy (represented by SCR, which is ignored if $a = 0$). If $a = 0$ and there is no storage (Figure 26b), the south orientation is combined with east and west, since just south leads to surplus energy that does not contribute to demand coverage. The presence of storage (Figures 26d, 26f, 26h and 26j) allows to self-consume more of the PV energy produced by south, which is the orientation that yields the highest PV production (see Figure 23), contributing more effectively (with less PV capacity) to demand coverage than east or west. This is why more and more is installed in south as the battery capacity increases, to maximize SSR. North surfaces are totally disregarded by the solver because it is the orientation that yields the lowest PV production. This previous analysis was for $a = 0$. The following analysis is done for $a > 0$.

As the a value increases, and hence SCR starts having more and more weight in the optimization, the solver starts to reduce greatly the amount of modules placed in south orientation, since it leads to too much surplus energy. West and north orientations start to be prominent and combined with south orientation in the case of having a battery storage (Figures 26d, 26f, 26h and 26j). If there is no storage (Figure 26b), the solver chooses not to install in north (just a bit when $a = 0.25$), combining only south, east and west. Figure 29 and Figure 30 help understanding these solutions suggested by the solver. For practical reasons, Figure 30 is only shown for a tilt angle of 60°, which is the main tilt angle chosen by the solver, as discussed previously. Moreover, Figure 30 just shows results for no storage and for a battery capacity of 1 kWh/kWp, instead for the five battery capacities considered in the whole optimization problem. This is intended to help the understanding of the figures.

Figure 30 shows the evolution of SCR, SSR and EBI with PV capacity if this PV capacity is installed solely in one orientation. It is observed how north oriented modules lead to the highest SCR and the lowest SSR, both with and without storage. The lower SSR by north orientation is simply because the PV production is lower, as observed in Figure 23. However, most of this PV production is self-consumed, leading to small amounts of surplus energy and hence higher levels of SCR. This fact is because the lower the PV production

the more likely is that it covers some electricity demand without any excess energy, but it is also attributed to the smoother PV production profile of north surfaces compared to any other orientations, which can be observed in Figure 29a and Figure 29b. When the SSR threshold levels (clearly observed in Figures 30c and 30d) are reached for high PV output orientations, such as south, north surfaces offer the possibility to still cover the remaining electricity demand (not covered by south PV production) with small amounts of surplus energy, again, due to the smooth profile observed in Figure 29a and 29b. East surfaces, although they cover electricity demand in early morning hours (unlike south), are discarded by the solver to be combined with south orientation since it is a rather abrupt profile as well, which leads to much surplus energy. West surfaces cover electricity demand in later evening hours (unlike south) and is a much smoother profile than east, so are chosen by the solver in many scenarios to be combined with south and north (see Figure 26).

With no battery storage (Figure 26b), the solver chooses not to install in north surfaces probably because the SCR levels are not sufficiently high to counteract the low levels of SSR (Figures 30a and 30c). However, having a battery storage (Figures 26d, 26f, 26h and 26j) rises the SCR and SSR levels for all orientations (Figures 30b and 30d). North surfaces reach so high levels of SCR that the solver decides to install on this orientation, despite the lower levels of SSR. This lack of SSR levels is covered with south-oriented modules. West-oriented modules, which are in a middle-point between south and north in terms of SCR and SSR, are frequently combined with south and north, as already mentioned in the previous paragraph. It is interesting to see in Figure 30e how south and east lead to higher levels of EBI, but only until a certain PV capacity (40-50 houses). This is because these orientations yield a higher PV energy output which, for not too large PV capacities, is used effectively to cover the electricity demand (high SSR) with not too much surplus energy (high SCR). Since EBI penalises both grid exports and imports, aiming for high SCR and high SSR levels, EBI levels are higher for these orientations until the mentioned PV capacity. From this PV capacity on, the PV production from these orientations have achieved a maximum load-match (SSR threshold), causing more and more surplus energy, while west and north still contribute to electricity demand coverage with small surplus energy, because of their lower PV production and also smoother PV production profile.

It is worth discussing why in Figure 26 in the case of storage (Figures 26d, 26f, 26h and 26j) the orientations chosen by the solver are only south + north if $a = 0.25$ whereas west is also considered for higher a values. For $a = 0.25$ the solver decides to cover all houses with PV, whereas from this a value on, the PV installed capacity decreases drastically to ensure high values of SCR. If $a = 0.25$ there is little or no PV capacity constraint to prevent SCR levels from being low, hence a large PV capacity in north orientation is optimal since its smooth PV production profile allows to cover fairly well the load consumption profile, achieving high SSR levels while still achieving reasonable levels of SCR (according to $a = 0.25$). PV production from south is still suggested to increase the SSR. But the fact that there is a large PV capacity to ensure high SSR leads to large amounts of surplus energy (low SCR), which is reasonable for the optimization algorithm since the weight given to SCR is just $a = 0.25$. This same reasoning applies as well to the scenarios with storage in Figure 28, when maximizing $f_2 = EBI$, where the solver does not suggest to cover all 100 houses fully with PV, but around 60 houses, which is still a rather large PV capacity, large enough to ensure that the low PV production by north surfaces is counteracted with a large PV capacity (plus the contribution from the south-oriented modules). In this figure it is additionally observed how the installation in south increases as the PV capacity increases, since the surplus energy produced by south can be handled with an increasing battery capacity and be used to cover the electricity demand.

Back to Figure 26 in the case of storage (Figures 26d, 26f, 26h and 26j), when the a value in-

creases from $a = 0.25$ on, giving more weight to SCR in the optimization, the solver decides to decrease drastically the PV installed capacity, to around 20 houses fully covered with PV. In this case, north and south are combined with other orientation/tilt combinations, mainly with a tilt of 60° and a west orientation. This is because the low installed PV capacity to ensure high levels of SCR enables to install PV on a higher PV output orientation than north, whose energy production will be used for electricity demand coverage. This is why for $a > 0.25$ (traduced into low installed PV capacities) the solver suggests west to join the south + north orientation suggested if $a = 0.25$ (traduced into large installed PV capacities).

Finally, it is deemed very convenient to mention the work made by Freitas et al. [34], who perform a very similar study to the one presented in this report. In an energy sharing context, they develop a PV sizing approach that maximizes the SSR and minimizes the 'net-load variance', which is rather equivalent to the two objective functions considered in this report, which maximize SSR and SCR using weights (f_1), and maximize EBI (f_2). Under these optimization conditions, basically maximizing at the same time the electricity demand coverage with PV energy and the grid stability, they find that north-west surfaces are generously covered with PV and combined with other higher PV output orientations: "It is worth noting that in both façades and rooftops the slots belonging to north-west azimuths are fully occupied, which would be counter-intuitive if the adjustment of PV production to the demand profile was not considered".

Their study is based in Lisbon, Portugal (38°N 9°W), which is a location at a much lower latitude than the one considered in this report: Harstad, Norway (68°N 16°E). They argue that the PV installation on north-west surfaces is useful because of the load-match and the enlarged solar azimuth in Summer: "The fact that there is an increase in the electricity consumption in the morning and in the late afternoon biases the optimal systems towards such azimuths, so that high net load variance can be avoided and the PV produced electricity be self-consumed. This is particularly relevant in the summer when the solar path is enlarged and the sunshine rays can hit north facing surfaces in the blocks' location". Indeed, this fact is more noticeable the more northerly is the location, since the solar path is more enlarged in Summer months the higher the latitude. However, although this is of course a required condition for especially north surfaces to be valuable, it is not only about how much the solar azimuth enlarges in Summer, but about the smoother PV production profiles from north and west orientations than east and south. The higher SSR levels achieved with the energy produced by the south surfaces for low installed capacities, combined with the higher SCR levels achieved with the energy produced by west and north surfaces, can lead to high levels of electricity demand coverage with PV energy (high SSR) and low surplus energy (high SCR), enhancing the grid stability (high EBI).

6.4 Results validation

The results provided in Chapter 6.1 are subject to sources of error in two ways: first, in the functioning of the Excel model itself, meaning the modeling equations that calculate the inflows and outflows of energy (to/from battery, to/from load, to/from grid); second, in the degree of accuracy of the solutions provided by the "GRG Nonlinear with multistart" when solving the optimization problem to find the optimal PV capacities for each orientation/tilt combination. This chapter aims to cover both aspects: Figure 31 covers the former and Figure 32 covers the latter.

Figure 31 shows the relative difference in E_{SS} between using the developed Excel model, for a certain PV and battery capacities, and running SAM for the same PV and battery capacities. E_{SS} represents the PV energy (AC energy) that is used to meet the load consumption, either directly or through previous storage (see Equation 11). This relative

difference is calculated for two different scenarios, meaning two different PV and battery capacities, as described by Table 6. The first one, shown in blue color in Figure 31, corresponds to the optimal PV capacity solution when maximizing the objective function f_1 with $a = 0.25$ and a battery capacity of 1 kWh/kWp. The second one, shown in orange color in Figure 31, corresponds to the optimal PV capacity solution when maximizing the objective function f_2 and a battery capacity of 1 kWh/kWp. The optimal PV capacities for these two scenarios are shown graphically in Figure 26j (for $a = 0.25$) and Figure 28b (for 1 kWh/kWp), respectively.

Table 6: PV capacities from the Excel solver for the blue and orange scenarios shown in Figure 31. Both scenarios have a battery capacity of $1kWh/kWp$.

	Blue scenario	**Orange scenario**
60° South	55.66 houses (4501.96 kWp)	21.86 houses (1768.08 kWp)
60° North	44.34 houses (3586.44 kWp)	30.50 houses (2466.75 kWp)
20° East	-	2.88 houses (123.82 kWp)

These PV/battery capacities lead in the Excel model to certain values of E_{SS} for each time step, which are then compared (via relative difference) to the E_{SS} values calculated by SAM when inputting in SAM the same PV and battery capacities. For both scenarios, blue and orange, it is observed that the relative difference is very small for most of the 8760 hourly time-steps in the year. The mean relative difference (average value of the absolute values of the 8760 relative differences) is only 0.10% for the blue scenario and 0.17% for the orange scenario. These results, although they are just for two scenarios, show the rather high reliability of the Excel model when computing the flows of energy, starting from a certain installed PV/battery capacity and calculating the inflows/outflows of the battery, the energy delivered to the loads and the energy imported/exported from the grid. Finally, it must be noted that since SAM does not provide explicit values of E_{SS}, these have been calculated by adding up two metrics: "Electricity to load from battery AC" and "Electricity to load from system AC".

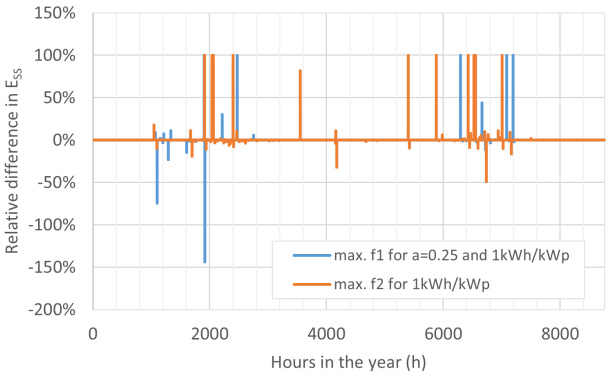

Figure 31: Relative difference in E_{SS} between the Excel model and SAM results. Two different scenarios are tested (see Table 4 for an overview of all scenarios).

Although the Excel model seems to be relatively reliable in terms of flows of energy, it is still uncertain and more difficult to validate the reliability of the optimal solutions (PV capacities) found by the "GRG Nonlinear with multistart" Excel solver, which is the one used to obtain all results in Chapter 6.1. The Excel model has been developed progressively, starting with just a few time-steps and decision variables to be able to determine at first sight whether the optimal solutions found by the solver are reasonable or not. Several

verification runs have been done when the model was fully completed as well.

The total PV capacity installed, SCR, SSR and EBI curves presented in Chapter 6.1 for the different scenarios (increasing the a weight when maximizing f_1 or increasing the battery capacity when maximizing f_1 or f_2) seem to follow a fitness logic, as tried to explain when discussing the results. Moreover, 30 different scenarios have been run to obtain all the results presented in Chapter 6.1 (see Table 4 for an overview of all scenarios). For each of these scenarios, the Excel solver is "reset" and run again. The "multistart" option starts from different points (possible solutions) each time the solver is run. The fact that the solver has been run multiple times (as a result of considering multiple scenarios), the "multistart" characteristics, and the fitness logic observed for the overall curves, add a certain degree of reliability to the optimal solutions found by the solver.

If it is assumed that the total PV capacity installed, SCR, SSR and EBI curves are reliable, it is likely that the the orientations/tilts suggested by the solver are reliable too. There are some solutions suggested by the solver that are rather intuitive, such as the scenarios for which the objective function is f_1 and $a = 0$, which means that all weight is given to cover the demand with PV energy regardless of the excess energy. In Figure 26 (right graphs), for $a = 0$ and any battery capacity, the solver chooses to cover all houses with PV and mostly or entirely in south with a tilt of 60°, which makes sense since it is the combination that yields the largest PV output in kWh/m^2 (see Figure 23). Furthermore, again, for $a = 0$ and any battery capacity, the PV installation in south with a tilt of 60° is more dominant the larger the battery capacity, which is also rather logical since the larger the battery storage capacity the easier becomes to self-consume the surplus energy from the south-oriented modules. This is also observed in Figure 28b when maximizing f_2.

The GRG solving method has the drawback of being easily trapped in local optimal solutions as explained in Chapter 4.6. This issue can be considerably mitigated when using different starting points, which Excel does by using the "multistart" option. In any case, six scenarios have been run using the "Evolutionary" solving method, which uses a different, more reliable but slower searching algorithm (see Chapter 4.6), to compare the results to those obtained in Chapter 6.1, which are all result of using the "GRG Nonlinear with multistart" solving method. The relative difference in SCR, SSR and EBI between solving these scenarios with "GRG Nonlinear with multistart" and "Evolutionary" is shown in Figure 32. It is observed that the optimal solutions found by Excel are similar regardless of which solving method is selected, since the relative differences are not higher than 2.5% for any of the six scenarios considered in Figure 32. These results show that two different optimization solving algorithms lead to very similar results, which adds reliability to the results obtained in Chapter 6.1.

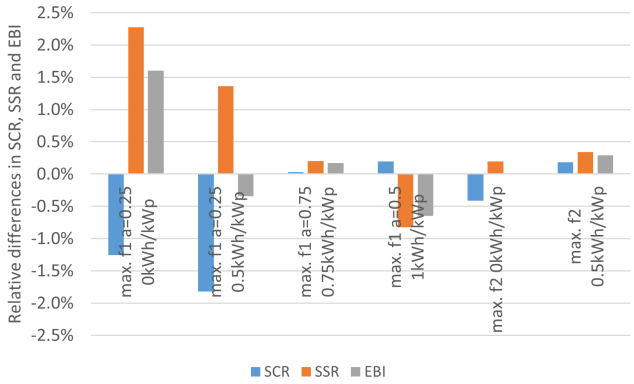

Figure 32: Relative difference in SCR, SSR and EBI between using the Excel solver "GRG Nonlinear with multistart" (the one used to obtain all results in Chapter 6.1) and the "Evolutionary" solver. Six different scenarios are tested (see Table 4 for an overview of all scenarios).

7 Conclusion and future work

7.1 Conclusion

In this report a PV sizing optimization model is developed in Excel, using as input PV generation data from the software SAM and load consumption data from the software Load Profile Generator. The Excel solver "GRG Nonlinear with multistart" is used to find the optimal PV capacities for certain battery capacity sizes and energy goals based on self-consumption metrics, such as the self-consumption rate (SCR), the self-sufficiency rate (SSR) and the energy balance index (EBI). The model is applied to an upcoming residential PV EC formed by 100 households in Harstad, Norway. The model developed is validated in terms of inflows and outflows of energy (to/from battery, to/from load, to/from grid) by comparing the model results with results from SAM, for arbitrary installed PV/battery capacities in the specific location. The optimal PV capacities solutions provided by the "GRG Nonlinear with multistart" Excel solver are validated by solving the optimization problem with another Excel solver, the "Evolutionary" solver, which uses a totally different solving algorithm than "GRG Nonlinear".

The following conclusions can be taken from this work:

- Optimal EC PV sizing must consider all possible surfaces with different orientations and tilts. Due to the specific Nordic location, a steep tilt of 60° (among 0°, 20°, 40° and 60°) is preferred because it leads to a larger and more uniform PV production throughout the year, larger than lower tilts in Winter and lower than lower tilts in Summer, which matches better the load consumption profile. All different orientations considered in the optimization problem (E,W,S,N) are used for optimal PV installation.

- South, west and east surfaces are frequently combined if there is no storage, whereas north surfaces start to be used if there is battery storage, and combined with south and west surfaces. A north orientation leads to much less PV generation but with a much smoother profile, especially than south and east, but also than west. High levels of electricity demand coverage (high SSR) are achieved with low PV capacities on high PV output orientations, such as south, but when a considerably high load-match has been achieved for the PV energy produced from these high PV output orientations, it is reasonable to cover the remaining electricity demand with PV energy from north and west orientations, causing small amounts of surplus energy (high SCR).

- Around 15-20 (out of the 100 forming the whole EC) houses with their roof fully covered with PV seems to be optimal if the goal is to find an optimal balance between SCR and SSR. This PV capacity, with its respective optimal orientation/tilt distribution, leads to an electricity demand coverage with PV energy (SSR) of around 15-20% and a self-consumption of the PV energy (SCR) close to 100%. If the goal is to maximize the grid stability (EBI), around 40-60 houses with their roof fully covered with PV seems to be optimal. This PV capacity, with its respective optimal orientation/tilt distribution, leads to an EBI of around 40-50%. Here, the exact numbers depend on the battery capacity and energy goals.

- Having a non-smart battery storage (charges whenever there is excess of PV energy and discharges whenever there is lack of PV energy) rises the SSR and EBI levels while keeping at similar levels the SCR. However, the increase in SSR and EBI is not too large and it seems to reach a threshold for a battery capacity of 0.75 kWh/kWp.

7.2 Future work

The work done in this report can be improved and extended in many different ways, such as:

- Considering higher time resolution data than hourly would give more accurate results. Jiménez-Castillo et al. [85] state: "In a household there may be high power fluctuations which may last from a few seconds to a few minutes. If averaged, these fluctuations may be flattened or they may even disappear if the recording interval is considerably larger. However, it must be highlighted that the load consumption provided from smart meters by most electricity distribution companies is generally between 15 min and 1 h and it depends on the type of customers". Cao and Sirén [99] state: "When using the coarser resolution, the averaging effect on both the generation and the demand will cause the matching capability to be overestimated".
- Instead of generating load profiles, considering real load profiles would add reliability to the results. Awad and Gül [64] state: "One of the primary challenges for designing the solar PV system for future communities which are not built yet is that the consumption data is not yet available". Fina et al. [59] state: "Although PV could in principle be installed according to a larger plan that ensures that the resulting solar electricity generation matches the demand profile of the PV host buildings, this is a challenging task to realize because the consumer behavior cannot be trivially inferred. Actual household consumption profiles are complex, featuring high variability and many spikes, which are difficult to grasp and model in a fully reliable way".
- The battery model developed could be improved by considering for instance a dependency between the battery operating voltage and the state of charge, leading to storage losses that have been disregarded.
- Different smart operating management systems could be included in the battery model, such as a load shifting strategy or one that maximizes self-sufficiency. The battery was assumed to be non-smart. Huang et al. [60] state: "The effect of storage is strongly influenced by its sizing and operating strategy".
- A PV inverter model could be developed as well to consider any thermal or clipping losses for instance. The inverter has just been considered by using a constant operating efficiency.
- The metric used to measure the grid stability, Energy Balance Index (EBI), defined by Hutty et al. [19], could be enhanced by penalising more strictly the grid import/export peaks. Freitas et al. [34] use, for instance, the root-mean-square deviation (RMSD) of the 'net-load variance' metric. The EBI metric was chosen mainly because it is a percentage metric.
- Discrete numbers have been considered to create the different scenarios; for instance, 5 values for the a value (and hence same for the b value), 5 battery capacity values, 4 different tilt angles, 4 different orientation angles, etc. Considering more values for each parameter or a range of values would give more accurate results.
- Using an alternate and more powerful optimization software than Excel [86] might also be convenient, especially if the problem is extended with sub-hourly time-steps or separate multi-objective functions.

It would be interesting and deemed as necessary to include economic metrics in the optimization algorithm. This has not been done due to a lack of time to find realistic economic data, as well as to perform a deep sensitivity analysis to cover different possible future

economic scenarios. Henni et al. [20] state: "It is important to carefully choose the regulatory framework when investigating the potential benefits of a sharing economy model". PV systems lifetimes are usually 25-30 years. Finding or making electricity prices predictions, including feed-in tariffs to give economic value to surplus PV energy, for this much time is challenging, as well as estimating other important economic parameters, such as the inflation rate or the discount rate [13]. However, this study should be done to give an economic perspective to complement the energy-related results found in this report.

The PV sizing optimization model developed has been specifically applied to an upcoming EC in Harstad, Norway, but can be understood as a generic tool to optimize the PV sizing in different locations and using different optimization objective functions and constraints.

References

[1] EU. What is an energy community?, December 2022. URL https://rural-energy-community-hub.ec.europa.eu/energy-communities/what-energy-community_en. [Online; accessed 19. Dec. 2022].

[2] Grønlia. Grønlia, May 2023. URL https://www.gronliaboligpark.no. [Online; accessed 3. May 2023].

[3] USGCRP. Global Temperature and Carbon Dioxide | GlobalChange.gov, June 2023. URL https://www.globalchange.gov/browse/multimedia/global-temperature-and-carbon-dioxide. [Online; accessed 5. Jun. 2023].

[4] NOAA. Annual 2022 Global Climate Report | National Centers for Environmental Information (NCEI), June 2023. URL https://www.ncei.noaa.gov/access/monitoring/monthly-report/global/202213#gtemp. [Online; accessed 5. Jun. 2023].

[5] UN, 2015. URL https://unfccc.int/sites/default/files/english_paris_agreement.pdf. [Online; accessed 24. Oct. 2022].

[6] UN, November 2021. URL https://ukcop26.org/wp-content/uploads/2021/11/COP26-Presidency-Outcomes-The-Climate-Pact.pdf. [Online; accessed 22. Mar. 2023].

[7] IPCC, October 2022. URL https://report.ipcc.ch/ar6/wg2/IPCC_AR6_WGII_FullReport.pdf. [Online; accessed 22. Mar. 2023].

[8] EU, January 2020. URL https://www.europarl.europa.eu/doceo/document/TA-9-2020-0005_EN.pdf. [Online; accessed 24. Oct. 2022].

[9] EU, June 2021. URL https://eur-lex.europa.eu/legal-content/EN/TXT/PDF/?uri=CELEX:32021R1119&from=EN. [Online; accessed 25. Oct. 2022].

[10] ClimateWatch. Net-zero Target Status, March 2023. URL https://www.climatewatchdata.org/net-zero-tracker?category=target_description&indicator=nz_status&showEUCountries=true. [Online; accessed 22. Mar. 2023].

[11] IEA, February 2023. URL https://iea-pvps.org/wp-content/uploads/2023/02/PVPS_Trend_Report_2022.pdf. [Online; accessed 22. Mar. 2023].

[12] IEA, November 2022. URL https://iea.blob.core.windows.net/assets/830fe099-5530-48f2-a7c1-11f35d510983/WorldEnergyOutlook2022.pdf. [Online; accessed 22. Mar. 2023].

[13] Johannes Radl, Andreas Fleischhacker, Frida Huglen Revheim, Georg Lettner, and Hans Auer. Comparison of profitability of pv electricity sharing in renewable energy communities in selected european countries. *Energies*, 13, 10 2020. ISSN 19961073. doi: 10.3390/en13195007.

[14] EU, December 2018. URL https://eur-lex.europa.eu/legal-content/EN/TXT/PDF/?uri=CELEX:32018L2001. [Online; accessed 25. Oct. 2022].

[15] EU, March 2019. URL https://eur-lex.europa.eu/legal-content/EN/TXT/PDF/?uri=CELEX:32019L0944. [Online; accessed 23. Mar. 2023].

[16] IEA, January 2023. URL https://iea-pvps.org/wp-content/uploads/2023/01/Report-IEA-PVPS-T16-04-2023-Firm-Power-generation.pdf. [Online; accessed 16. Mar. 2023].

[17] Rasmus Luthander, Joakim Widén, Daniel Nilsson, and Jenny Palm. Photovoltaic self-consumption in buildings: A review. *Applied Energy*, 142:80–94, 3 2015. ISSN 03062619. doi: 10.1016/J.APENERGY.2014.12.028.

[18] Ruchi Gupta, Alejandro Pena-Bello, Kai Nino Streicher, Cattia Roduner, Yamshid Farhat, David Thöni, Martin Kumar Patel, and David Parra. Spatial analysis of distribution grid capacity and costs to enable massive deployment of PV, electric mobility and electric heating. *Appl. Energy*, 287: 116504, April 2021. ISSN 0306-2619. doi: 10.1016/j.apenergy.2021.116504.

[19] Timothy D. Hutty, Alejandro Pena-Bello, Siyuan Dong, David Parra, Rachael Rothman, and Solomon Brown. Peer-to-peer electricity trading as an enabler of increased pv and ev ownership. *Energy Conversion and Management*, 245, 10 2021. ISSN 01968904. doi: 10.1016/j.enconman.2021.114634.

[20] Sarah Henni, Philipp Staudt, and Christof Weinhardt. A sharing economy for residential communities with pv-coupled battery storage: Benefits, pricing and participant matching. *Applied Energy*, 301, 11 2021. ISSN 03062619. doi: 10.1016/j.apenergy.2021.117351.

[21] Vladimir Z. Gjorgievski, Snezana Cundeva, and George E. Georghiou. Social arrangements, technical designs and impacts of energy communities: A review. *Renewable Energy*, 169:1138–1156, 5 2021. ISSN 18790682. doi: 10.1016/J.RENENE.2021.01.078.

[22] Fuyou Zhao, Zhenpeng Li, Dengjia Wang, and Tao Ma. Peer-to-peer energy sharing with demand-side management for fair revenue distribution and stable grid interaction in the photovoltaic community. *Journal of Cleaner Production*, 383, 1 2023. ISSN 09596526. doi: 10.1016/J.JCLEPRO.2022.135271.

[23] BMG. Brooklyn Microgrid | Community Powered Energy, March 2023. URL https://www.brooklyn.energy. [Online; accessed 20. Mar. 2023].

[24] Esther Mengelkamp, Johannes Gärttner, Kerstin Rock, Scott Kessler, Lawrence Orsini, and Christof Weinhardt. Designing microgrid energy markets: A case study: The brooklyn microgrid. *Applied Energy*, 210:870–880, 1 2018. ISSN 03062619. doi: 10.1016/J.APENERGY.2017.06.054.

[25] L Ableitner, A Meeuw, S Schopfer, V Tiefenbeck, F Wortmann, and A Wörner. Quartierstrom-implementation of a real world prosumer centric local energy market in walenstadt, switzerland. 2019.

[26] Sonnen. sonnenCommunity | sonnen, March 2023. URL https://sonnengroup.com/sonnencommunity. [Online; accessed 20. Mar. 2023].

[27] EU. Energy communities, November 2022. URL https://energy.ec.europa.eu/topics/markets-and-consumers/energy-communities_en. [Online; accessed 4. Nov. 2022].

[28] EU. Home, November 2022. URL https://energy-communities-repository.ec.europa.eu/index_en. [Online; accessed 4. Nov. 2022].

[29] EU. Home, November 2022. URL https://rural-energy-community-hub.ec.europa.eu/index_en. [Online; accessed 4. Nov. 2022].

[30] FH Salzburg. Mess-Infrastruktur und Datenanalyse für Local Energy Communities, November 2022. URL https://its.fh-salzburg.ac.at/projekte/studierendenprojekte/suche/mess-infrastruktur-und-datenanalyse-fuer-local-energy-communities. [Online; accessed 22. Nov. 2022].

[31] Mohammad Amin Vaziri Rad, Ashkan Toopshekan, Parisa Rahdan, Alibakhsh Kasaeian, and Omid Mahian. A comprehensive study of techno-economic and environmental features of different solar tracking systems for residential photovoltaic installations. *Renewable and Sustainable Energy Reviews*, 129, 9 2020. ISSN 18790690. doi: 10.1016/j.rser.2020.109923.

[32] Michael Hartner, André Ortner, Albert Hiesl, and Reinhard Haas. East to west - the optimal tilt angle and orientation of photovoltaic panels from an electricity system perspective. *Applied Energy*, 160:94–107, 12 2015. ISSN 03062619. doi: 10.1016/j.apenergy.2015.08.097.

[33] M. C. Brito, S. Freitas, S. Guimarães, C. Catita, and P. Redweik. The importance of facades for the solar pv potential of a mediterranean city using lidar data. *Renewable Energy*, 111:85–94, 2017. ISSN 18790682. doi: 10.1016/j.renene.2017.03.085.

[34] S. Freitas, C. Reinhart, and M. C. Brito. Minimizing storage needs for large scale photovoltaics in the urban environment. *Solar Energy*, 159:375–389, 1 2018. ISSN 0038092X. doi: 10.1016/j.solener.2017.11.011.

[35] EEA, August 2016. URL https://www.efta.int/media/documents/legal-texts/eea/the-eea-agreement/Main%20Text%20of%20the%20Agreement/EEAagreement.pdf. [Online; accessed 24. Mar. 2023].

[36] UNFCCC, November 2022. URL https://unfccc.int/sites/default/files/NDC/2022-11/NDC%20Norway_second%20update.pdf. [Online; accessed 24. Mar. 2023].

[37] Loftidend, March 2023. URL https://lovdata.no/static/lovtidend/ltavd1/2017/nl-20170616-060.pdf. [Online; accessed 24. Mar. 2023].

[38] Climate&Environment, July 2022. URL https://www.regjeringen.no/contentassets/a78ecf5ad2344fa5ae4a394412ef8975/en-gb/pdfs/stm202020210013000engpdfs.pdf. [Online; accessed 24. Mar. 2023].

[39] IEA, June 2022. URL https://iea.blob.core.windows.net/assets/de28c6a6-8240-41d9-9082-a5dd65d9f3eb/NORWAY2022.pdf. [Online; accessed 24. Mar. 2023].

[40] NVE. Kompensasjonsordning for høye strømpriser - NVE, January 2020. URL https://www.nve.no/reguleringsmyndigheten/nytt-fra-rme/nyheter-reguleringsmyndigheten-for-energi/kompensasjonsordning-for-hoeye-stroempriser. [Online; accessed 31. Mar. 2023].

[41] NVE, November 2021. URL https://publikasjoner.nve.no/rapport/2021/rapport2021_29.pdf. [Online; accessed 24. Mar. 2023].

[42] IEA, January 2023. URL https://iea-pvps.org/wp-content/uploads/2023/01/IEA-PVPS-T13-21-2022-REPORT-Soiling-Losses-PV-Plants.pdf. [Online; accessed 30. Mar. 2023].

[43] IEA, March 2022. URL https://iea-pvps.org/wp-content/uploads/2022/03/IEA-PVPS_Annual_Report_2021.pdf. [Online; accessed 16. Mar. 2023].

[44] IEA, April 2020. URL https://iea-pvps.org/wp-content/uploads/2019/10/NSR_Norway_2018.pdf. [Online; accessed 8. Mar. 2023].

[45] Li He and Jie Zhang. A community sharing market with pv and energy storage: An adaptive bidding-based double-side auction mechanism. *IEEE Transactions on Smart Grid*, 12:2450–2461, 5 2021. ISSN 19493061. doi: 10.1109/TSG.2020.3042190.

[46] Zhenpeng Li and Tao Ma. Peer-to-peer electricity trading in grid-connected residential communities with household distributed photovoltaic. *Applied Energy*, 278, 11 2020. ISSN 03062619. doi: 10.1016/j.apenergy.2020.115670.

[47] Alejandro Nuñez-Jimenez, Prakhar Mehta, and Danielle Griego. Let it grow: How community solar policy can increase pv adoption in cities. *Energy Policy*, 175, 4 2023. ISSN 03014215. doi: 10.1016/J.ENPOL.2023.113477.

[48] Jiatong Wang, Jiangfeng Zhang, Li Li, and Yunfeng Lin. Peer-to-peer energy trading for residential prosumers with photovoltaic and battery storage systems. *IEEE Systems Journal*, 2022. ISSN 19379234. doi: 10.1109/JSYST.2022.3190976.

[49] Liaqat Ali, S. M. Muyeen, Arindam Ghosh, and Hamed Bizhani. Optimal sizing of networked microgrid using game theory considering the peer-to-peer energy trading. pages 322–326, 2020. doi: 10.1109/SPIES48661.2020.9243067.

[50] Xu Xu, Jiayong Li, Yan Xu, Zhao Xu, and Chun Sing Lai. A two-stage game-theoretic method for residential pv panels planning considering energy sharing mechanism. *IEEE Transactions on Power Systems*, 35:3562–3573, 9 2020. ISSN 15580679. doi: 10.1109/TPWRS.2020.2985765.

[51] Yuwei Yang, Changming Lu, Hao Liu, Nan Wang, Lian Chen, Chenchen Wang, Xudong Jiang, and Cheng Ye. Optimal design and energy management of residential prosumer community with photovoltaic power generation and storage for electric vehicles. *Sustainable Production and Consumption*, 33:244–255, 9 2022. ISSN 23525509. doi: 10.1016/J.SPC.2022.07.008.

[52] Gianfranco Di Lorenzo, Sara Rotondo, Rodolfo Araneo, Giovanni Petrone, and Luigi Martirano. Innovative power-sharing model for buildings and energy communities. *Renewable Energy*, 172:1087–1102, 7 2021. ISSN 18790682. doi: 10.1016/j.renene.2021.03.063.

[53] Yasin Zabihinia Gerdroodbari, Reza Razzaghi, and Farhad Shahnia. Improving voltage regulation and unbalance in distribution networks using peer-to-peer data sharing between single-phase pv inverters. *IEEE Transactions on Power Delivery*, PP:1–1, 09 2021. doi: 10.1109/TPWRD.2021.3113011.

[54] Prakhar Mehta and Verena Tiefenbeck. Solar pv sharing in urban energy communities: Impact of community configurations on profitability, autonomy and the electric grid. *Sustainable Cities and Society*, 87, 12 2022. ISSN 22106707. doi: 10.1016/J.SCS.2022.104178.

[55] Jiaming Li. Optimal sizing of grid-connected photovoltaic battery systems for residential houses in australia. *Renewable Energy*, 136:1245–1254, 6 2019. ISSN 18790682. doi: 10.1016/J.RENENE.2018.09.099.

[56] Bernadette Fina, Andreas Fleischhacker, Hans Auer, and Georg Lettner. Economic assessment and business models of rooftop photovoltaic systems in multiapartment buildings: Case studies for austria and germany. *Journal of Renewable Energy*, 2018:1–16, 2018. ISSN 2314-4386. doi: 10.1155/2018/9759680.

[57] Verena Heinisch, Mikael Odenberger, Lisa Göransson, and Filip Johnsson. Organizing prosumers into electricity trading communities: Costs to attain electricity transfer limitations and self-sufficiency goals. *International Journal of Energy Research*, 43:7021–7039, 10 2019. ISSN 1099114X. doi: 10.1002/ER.4720.

[58] Abdurahman Yaldız, Tayfur Gökçek, İbrahim Şengör, and Ozan Erdinç. Optimal sizing and economic analysis of photovoltaic distributed generation with battery energy storage system considering peer-to-peer energy trading. *Sustainable Energy, Grids and Networks*, 28, 12 2021. ISSN 23524677. doi: 10.1016/J.SEGAN.2021.100540.

[59] Bernadette Fina, Hans Auer, and Werner Friedl. Profitability of pv sharing in energy communities: Use cases for different settlement patterns. *Energy*, 189, 12 2019. ISSN 03605442. doi: 10.1016/j.energy.2019.116148.

[60] Pei Huang, Yongjun Sun, Marco Lovati, and Xingxing Zhang. Solar-photovoltaic-power-sharing-based design optimization of distributed energy storage systems for performance improvements. *Energy*, 222, 5 2021. ISSN 03605442. doi: 10.1016/j.energy.2021.119931.

[61] Susana Soeiro and Marta Ferreira Dias. Renewable energy community and the european energy market: main motivations. *Heliyon*, 6, 7 2020. ISSN 24058440. doi: 10.1016/J.HELIYON.2020.E04511.

[62] Florian Hanke, Rachel Guyet, and Marielle Feenstra. Do renewable energy communities deliver energy justice? exploring insights from 71 european cases. *Energy Research and Social Science*, 80, 10 2021. ISSN 22146296. doi: 10.1016/J.ERSS.2021.102244.

[63] Theresia Perger, Lukas Wachter, Andreas Fleischhacker, and Hans Auer. Pv sharing in local communities: Peer-to-peer trading under consideration of the prosumers' willingness-to-pay. *Sustainable Cities and Society*, 66, 3 2021. ISSN 22106707. doi: 10.1016/j.scs.2020.102634.

[64] Hadia Awad and Mustafa Gül. Optimisation of community shared solar application in energy efficient communities. *Sustainable Cities and Society*, 43:221–237, 11 2018. ISSN 22106707. doi: 10.1016/j.scs.2018.08.029.

[65] ScienceDirect. Solar Altitude Angle - an overview | ScienceDirect Topics, November 2022. URL https://www.sciencedirect.com/topics/engineering/solar-altitude-angle. [Online; accessed 22. Nov. 2022].

[66] Benjamin Y.H. Liu and Richard C. Jordan. The long-term average performance of flat-plate solar-energy collectors. with design data for the u.s., its outlying possessions and canada. *Solar Energy*, 7:53–74, 1963. ISSN 0038092X. doi: 10.1016/0038-092X(63)90006-9.

[67] Douglas T. Reindl. Estimating diffuse radiation on horizontal surfaces and total radiation on tilted surfaces. 1988.

[68] Richard Perez, R. Stewart, R. Seals, and T. Guertin. The development and verification of the perez diffuse radiation model. 10 1988.

[69] NREL, March 2018. URL https://www.nrel.gov/docs/fy18osti/67399.pdf. [Online; accessed 22. Nov. 2022].

[70] PVeducation. IV Curve | PVEducation, November 2022. URL https://www.pveducation.org/pvcdrom/solar-cell-operation/iv-curve. [Online; accessed 22. Nov. 2022].

[71] W. De Soto, S. A. Klein, and W. A. Beckman. Improvement and validation of a model for photovoltaic array performance. *Solar Energy*, 80:78–88, 2006. ISSN 0038092X. doi: 10.1016/J.SOLENER.2005.06.010.

[72] Ty Neises, Sanford Klein, and Douglas Reindl. Development of a thermal model for photovoltaic modules and analysis of noct guidelines. *Journal of Solar Energy Engineering*, 134, 02 2012. doi: 10.1115/1.4005340.

[73] D L King, W E Boyson, and J A Kratochvil. Photovoltaic array performance model. 2004.

[74] PVPerformance. PV Performance Modeling Collaborative | Single Diode Equivalent Circuit Models, March 2023. URL https://pvpmc.sandia.gov/modeling-steps/2-dc-module-iv/diode-equivalent-circuit-models. [Online; accessed 30. Mar. 2023].

[75] Aron P. Dobos. An improved coefficient calculator for the california energy commission 6 parameter photovoltaic module model. *Journal of Solar Energy Engineering, Transactions of the ASME*, 134, 5 2012. ISSN 01996231. doi: 10.1115/1.4005759/455696. URL https://asmedigitalcollection.asme.org/solarenergyengineering/article/134/2/021011/455696/An-Improved-Coefficient-Calculator-for-the.

[76] Aron P. Dobos and Sara M. MacAlpine. Procedure for applying iec-61853 test data to a single diode model. pages 2846–2849, June 2014. ISSN 0160-8371. doi: 10.1109/PVSC.2014.6925525.

[77] Yash Kotak, Mehreen Gul, T. Muneer, and Stoyanka Ivanova. Investigating the impact of ground albedo on the performance of pv systems. 04 2015.

[78] Alex Gardner and Martin Sharp. A review of snow and ice albedo and the development of a new physically based broadband albedo parameterization. *Journal of Geophysical Research*, 115, 03 2010. doi: 10.1029/2009JF001444.

[79] IEA, January 2023. URL https://iea-pvps.org/wp-content/uploads/2022/11/IEA-PVPS-Report-T13-25-2022-0andM-Guidelines.pdf. [Online; accessed 12. Mar. 2023].

[80] Hadia Awad, Mustafa Gül, K. M Emtiaz Salim, and Haitao Yu. Predicting the energy production by solar photovoltaic systems in cold-climate regions. *International Journal of Sustainable Energy*, 37:978–998, 11 2018. ISSN 1478646X. doi: 10.1080/14786451.2017.1408622.

[81] Bill Marion, Robert Schaefer, Holden Caine, and Gonzalo Sanchez. Measured and modeled photovoltaic system energy losses from snow for colorado and wisconsin locations. *Solar Energy*, 97: 112–121, 11 2013. ISSN 0038092X. doi: 10.1016/J.SOLENER.2013.07.029.

[82] NREL, August 2017. URL https://www.nrel.gov/docs/fy17osti/68705.pdf. [Online; accessed 30. Mar. 2023].

[83] Helene Pedersen, Johann Strauss, and Josefine Selj. Effect of soiling on photovoltaic modules in norway. *Energy Procedia*, 92:585–589, 2016. ISSN 1876-6102. doi: https://doi.org/10.1016/j.egypro.2016.07.023. URL https://www.sciencedirect.com/science/article/pii/S1876610216304507. Proceedings of the 6th International Conference on Crystalline Silicon Photovoltaics (SiliconPV 2016).

[84] VelaSolaris, January 2022. URL https://www.velasolaris.com/wp-content/uploads/2022/01/Tutorial_EN.pdf. [Online; accessed 10. May 2023].

[85] G. Jiménez-Castillo, F. J. Muñoz-Rodriguez, C. Rus-Casas, and D. L. Talavera. A new approach based on economic profitability to sizing the photovoltaic generator in self-consumption systems without storage. *Renewable Energy*, 148:1017–1033, 4 2020. ISSN 18790682. doi: 10.1016/j.renene.2019.10.086.

[86] FrontlineSolvers. Excel Solver Online Help, September 2021. URL https://www.solver.com/excel-solver-online-help. [Online; accessed 11. Apr. 2023].

[87] P. E. Charlie Young. Excel Solver: Which Solving Method Should I Choose? - EngineerExcel. *EngineerExcel*, March 2021. URL https://engineerexcel.com/excel-solver-solving-method-choose.

[88] Anna Barry. ROOF PITCH FACTOR [How To Find & Use], April 2020. URL https://concalculator.com/blog/roof-pitch-factor. [Online; accessed 8. Apr. 2023].

[89] EUComission. JRC Photovoltaic Geographical Information System (PVGIS) - European Commission, November 2016. URL https://re.jrc.ec.europa.eu/pvg_tools/en. [Online; accessed 2. Apr. 2023].

[90] KlimaServiceCenter. Observations and weather statistics - Seklima, February 2023. URL https://seklima.met.no/observations. [Online; accessed 3. Apr. 2023].

[91] LoadProfileGenerator. LoadProfileGenerator, March 2023. URL https://www.loadprofilegenerator.de. [Online; accessed 4. Apr. 2023].

[92] Noah Pflugradt. Modellierung von wasser-und energieverbräuchen in haushalten. 2016.

[93] StatisticsNorway. Families and households. Statbank Norway, April 2023. URL https://www.ssb.no/en/statbank/list/familie. [Online; accessed 4. Apr. 2023].

[94] Runda, July 2020. URL https://cdn.energypal.com/panels/rs330s-120/energypal-solar-panel-spec-datasheet-runda-pv-rs320-335s-120-rs330s-120.pdf. [Online; accessed 10. May 2023].

[95] Giacomo Cillari, Alessandro Franco, and Fabio Fantozzi. Sizing strategies of photovoltaic systems in nzeb schemes to maximize the self-consumption share. *Energy Reports*, 7:6769–6785, 11 2021. ISSN 23524847. doi: 10.1016/j.egyr.2021.09.117.

[96] FrontlineSolvers. Excel Solver - Change Options for GRG Nonlinear Solving Method, April 2015. URL https://www.solver.com/excel-solver-change-options-grg-nonlinear-solving-method. [Online; accessed 10. May 2023].

[97] FrontlineSolvers. Excel Solver - Change Options for Evolutionary Solving Method, April 2016. URL https://www.solver.com/excel-solver-change-options-evolutionary-solving-method. [Online; accessed 10. May 2023].

[98] Hadia Awad, Mustafa Gül, and Mohamed Al-Hussein. Long-term performance and GHG emission offset analysis of small-scale grid-tied residential solar PV systems in northerly latitudes. *Adv. Build. Energy Res.*, 15(6):733–754, November 2021. ISSN 1751-2549. doi: 10.1080/17512549.2020.1720812.

[99] Sunliang Cao and Kai Sirén. Impact of simulation time-resolution on the matching of PV production and household electric demand. *Appl. Energy*, 128:192–208, September 2014. ISSN 0306-2619. doi: 10.1016/j.apenergy.2014.04.075.

[100] PVeducation. Air Mass | PVEducation, March 2023. URL https://www.pveducation.org/pvcdrom/properties-of-sunlight/air-mass. [Online; accessed 28. Mar. 2023].

Appendix

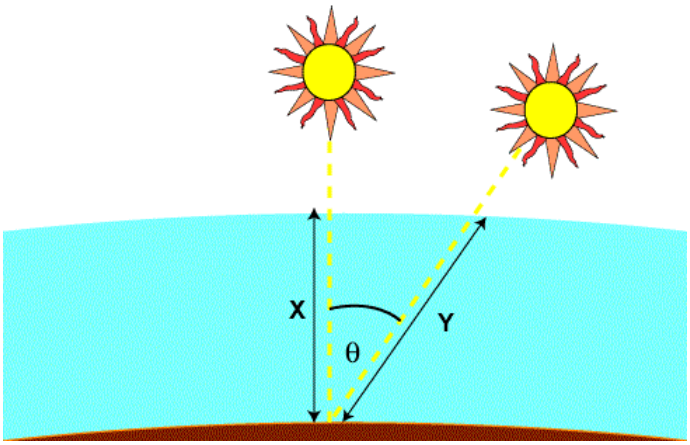

.

Figure 33: The blue color represents the atmosphere while the brown color represents the Earth's surface. In this figure $\theta = \theta_z$ since the light hits an horizontal plane. The air mass (AM) represents the proportion of atmosphere that the light must pass through before striking the Earth relative to its overhead path length, so $AM = Y/X = 1/cos(\theta_z)$. Since $\theta_z + \alpha_s = 90°$, $AM = Y/X = 1/sin(\alpha_s)$ [100].

(a) (b)

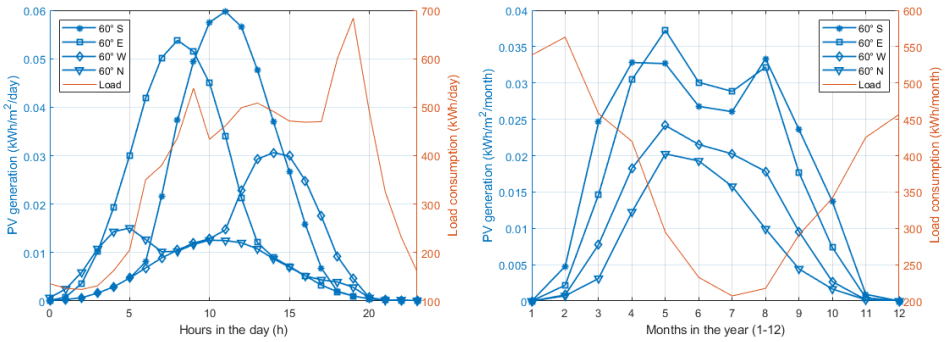

Figure 34: Daily (left graph) and monthly (right graph) averaged PV generation profiles (blue curves) and EC aggregated load consumption profile (red curve) for a tilt of 60° and the four different orientations considered (S,E,W and N). Nomenclature: for instance, "60° S" means a tilt of 60° and a south orientation.

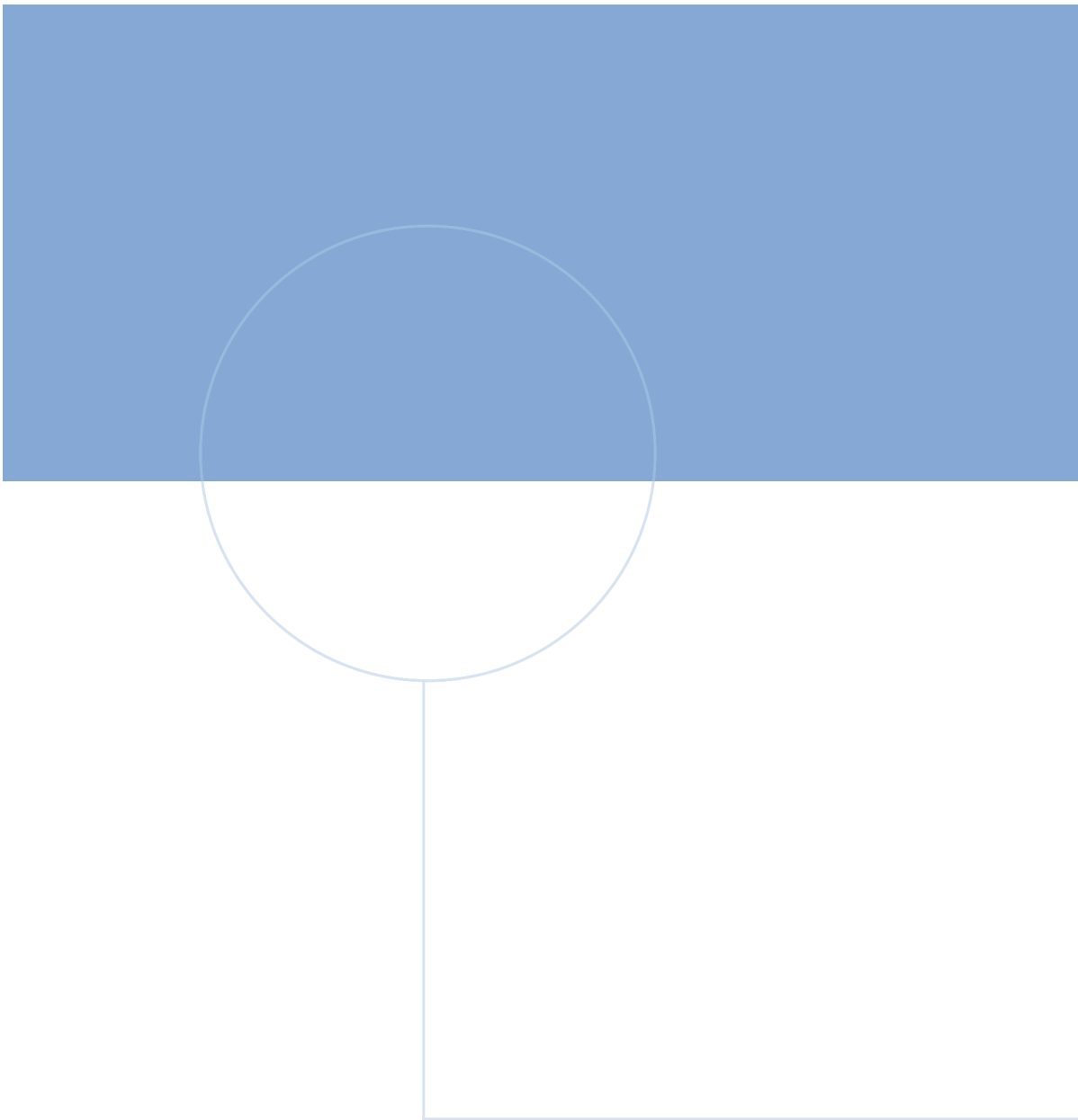

NTNU

Norwegian University of
Science and Technology